Why do Models Overestimate Surface Ozone in the Southeastern United States?

Katherine R. Travis[1], Daniel J. Jacob[1,2], Jenny A. Fisher[3,4], Patrick S. Kim[2], Eloise A. Marais[1], Lei Zhu[1], Karen Yu[1], Christopher C. Miller[1], Robert M. Yantosca[1], Melissa P. Sulprizio[1], Anne M. Thompson[5], Paul O. Wennberg[6,7], John D. Crounse[6], Jason M. St. Clair[6], Ronald C. Cohen[8], Joshua L. Laughner[8], Jack E. Dibb[9], Samuel R. Hall[10], Kirk Ullmann[10], Glenn M. Wolfe[11,12], Illana B. Pollack[13], Jeff Peischl[14,15], Jonathan A. Neuman[14,15], and Xianliang Zhou[16,17]

[1]Department of Earth and Planetary Sciences and School of Engineering and Applied Sciences, Harvard University, Cambridge, Massachusetts, USA
[2]Earth and Planetary Sciences, Harvard University, Cambridge, MA, USA
[3]Centre for Atmospheric Chemistry, School of Chemistry, University of Wollongong, Wollongong, NSW, Australia
[4]School of Earth and Environmental Sciences, University of Wollongong, Wollongong, NSW, Australia
[5]NASA Goddard Space Flight Center, Greenbelt, Maryland, USA
[6]Division of Geological and Planetary Sciences, California Institute of Technology, Pasadena, CA, USA
[7]Division of Engineering and Applied Science, California Institute of Technology, Pasadena, CA, USA
[8]Department of Chemistry, University of California, Berkeley, CA, USA
[9]Earth System Research Center, University of New Hampshire, Durham, NH, USA
[10]Atmospheric Chemistry Division, National Center for Atmospheric Research, Boulder, CO, USA
[11]Atmospheric Chemistry and Dynamics Laboratory, NASA Goddard Space Flight Center, Greenbelt, MD, USA
[12]Joint Center for Earth Systems Technology, University of Maryland Baltimore County, Baltimore, MD, USA
[13]Atmospheric Science Department, Colorado State University, Fort Collins, Colorado, USA
[14]University of Colorado, Cooperative Institute for Research in Environmental Sciences, Boulder, CO, USA
[15]NOAA, Division of Chemical Science, Earth Systems Research Lab, Boulder, CO USA
[16]Department of Environmental Health and Toxicology, School of Public Health, State University of New York at Albany, Albany, New York, USA
[17]Wadsworth Center, New York State Department of Health, Albany, New York, USA

Correspondence to: Katherine R. Travis (ktravis@fas.harvard.edu)

Abstract. Ozone pollution in the Southeast US involves complex chemistry driven by emissions of anthropogenic nitrogen oxide radicals ($NO_x \equiv NO + NO_2$) and biogenic isoprene. Model estimates of surface ozone concentrations tend to be biased high in the region and this is of concern for designing effective emission control strategies to meet air quality standards. We use detailed chemical observations from the SEAC^{4}RS aircraft campaign in August and September 2013, interpreted with the GEOS-Chem chemical transport model at 0.25°×0.3125° horizontal resolution, to better understand the factors controlling surface ozone in the Southeast US. We find that the National Emission Inventory (NEI) for NO_x from the US Environmental Protection Agency (EPA) is too high in the Southeast and nationally by a factor of 2. This finding is based on SEAC^{4}RS observations of NO_x and its oxidation products, surface network observations of nitrate wet deposition fluxes, and OMI satellite observations of tropospheric NO_2 columns. Upper tropospheric NO_2 from lightning makes a large contribution to the satellite observations that must be accounted for when using these data to estimate surface NO_x emissions. We find that only

half of isoprene oxidation proceeds by the high-NO_x pathway to produce ozone; this fraction is only moderately sensitive to changes in NO_x emissions because isoprene and NO_x emissions are spatially segregated. GEOS-Chem with reduced NO_x emissions provides an unbiased simulation of ozone observations from the aircraft, and reproduces the observed ozone production efficiency in the boundary layer as derived from a regression of ozone and NO_x oxidation products. However, the model is still biased high by 8±13 ppb relative to observed surface ozone in the Southeast US. Ozonesondes launched during midday hours show a 7 ppb ozone decrease from 1.5 km to the surface that GEOS-Chem does not capture. This may be caused by excessively dry conditions in the model, representing another factor important in the simulation of surface ozone.

1 Introduction

Ground-level ozone is a harmful air pollutant for human health and vegetation. Ozone is produced in the troposphere when volatile organic compounds (VOCs) and carbon monoxide (CO) are photochemically oxidized in the presence of nitrogen oxide radicals ($NO_x \equiv NO+NO_2$). The mechanism for producing ozone is complicated, involving hundreds of chemical species interacting with transport on all scales. In October 2015, the US Environmental Protection Agency (EPA) set a new National Ambient Air Quality Standard (NAAQS) for surface ozone as a maximum daily 8-h average (MDA8) of 0.070 ppm not to be exceeded more than three times per year. This is the latest in a succession of gradual tightening of the NAAQS from 0.12 ppm (1-h average) to 0.08 ppm in 1997, and to 0.075 ppm in 2008, responding to accumulating evidence that ozone is detrimental to public health even at low concentrations (EPA, 2013). Chemical transport models (CTMs) tend to significantly overestimate surface ozone in the Southeast US (Lin et al., 2008; Fiore et al., 2009; Reidmiller et al., 2009; Brown-Steiner et al., 2015; Canty et al., 2015). Here we examine why by using the GEOS-Chem CTM to simulate NASA SEAC^{4}RS aircraft observations of ozone and its precursors over the region in August-September 2013 (Toon et al., 2016), together with additional observations from surface networks.

A number of explanations have been proposed for the ozone model biases in the Southeast US. Fiore et al. (2003) suggested excessive modeled ozone inflow from the Gulf of Mexico. Lin et al. (2008) proposed that the ozone dry deposition velocity could be underestimated. McDonald-Buller et al. (2011) pointed out the potential role of halogen chemistry as a sink of ozone. Isoprene is the principal VOC precursor of ozone in the Southeast US in summer, and Fiore et al. (2005) found that a major source of uncertainty is the magnitude of isoprene emissions from vegetation and the loss of NO_x through formation of isoprene nitrates. Horowitz et al. (2007) found a large sensitivity of ozone to the fate of isoprene nitrates and the extent to which they release NO_x when oxidized. Squire et al. (2015) found that the choice of isoprene oxidation mechanism can alter both the sign and magnitude of the response of ozone to isoprene and NO_x emissions.

The SEAC^{4}RS aircraft campaign in August-September 2013 provided an outstanding opportunity to improve our understanding of ozone chemistry over the Southeast US. The SEAC^{4}RS DC-8 aircraft hosted an unprecedented chemical

payload including isoprene and its oxidation products, NO_x and its oxidation products, and ozone. The flights featured extensive boundary layer mapping of the Southeast as well as vertical profiling to the free troposphere (Toon et al., 2016). We use the GEOS-Chem global CTM with high horizontal resolution over North America (0.25°×0.3125°) to simulate and interpret the SEAC^{4}RS observations. We integrate into our analysis additional Southeast US observations during the summer of 2013 including the NOMADSS aircraft campaign, the SOAS surface site in Alabama, the SEACIONS ozonesonde network, the CASTNET ozone network, the NADP nitrate wet deposition network, and NO_2 satellite data from the OMI instrument. Several companion papers apply GEOS-Chem to simulate other aspects of SEAC^{4}RS and concurrent data for the Southeast US including aerosol sources and optical depth (Kim et al., 2015), isoprene organic aerosol (Marais et al., 2016), organic nitrates (Fisher et al., 2016), formaldehyde and its relation to satellite observations (Zhu et al., 2016), and sensitivity to model resolution (Yu et al., 2016).

2 GEOS-Chem Model Description

We use the GEOS-Chem global 3-D CTM (Bey et al., 2001) in version 9.02 (www.geos-chem.org) with modifications described below. GEOS-Chem is driven with assimilated meteorological data from the Goddard Earth Observing System – Forward Processing (GEOS-5.11.0) of the NASA Global Modeling and Assimilation Office (GMAO). The GEOS-5.11.0 data have a native horizontal resolution of 0.25° latitude by 0.3125° longitude and a temporal resolution of 3 h (1 h for surface variables and mixing depths). We use a nested version of GEOS-Chem (Chen et al., 2009) with native 0.25° × 0.3125° horizontal resolution over North America and adjacent oceans (130° - 60°W, 9.75° - 60°N) and dynamic boundary conditions from a global simulation with 4° × 5° horizontal resolution. Turbulent boundary layer mixing follows a non-local parameterization based on K-theory (Holtslag and Boville, 1993) implemented in GEOS-Chem by Lin and McElroy (2010). Daytime mixing depths are reduced by 40% as described by Kim et al. (2015) and Zhu et al. (2016) to match lidar observations of boundary layer height from SEAC^{4}RS. We conducted the GEOS-Chem nested model simulation for August-September 2013, following six months of initialization at 4° × 5° resolution.

2.1 Chemistry

The chemical mechanism in GEOS-Chem version 9.02 is described by Mao et al, (2010, 2013). Here, we have aerosol reactive uptake of HO_2 produce H_2O_2, instead of H_2O as in Mao et al. (2013), to better match H_2O_2 observations in SEAC^{4}RS. We include a number of updates to isoprene chemistry, listed comprehensively in the Supplementary Material (Tables S1 and S2) and describe here more specifically the low-NO_x pathways. Companion papers describe the updates relevant to isoprene nitrates (Fisher et al., 2016) and organic aerosol formation (Marais et al., 2016). Oxidation of biogenic monoterpenes was also added to the GEOS-Chem mechanism (Fisher et al., 2016) but does not significantly affect ozone.

A critical issue in isoprene chemistry is the fate of the isoprene peroxy radicals ($ISOPO_2$) produced from the oxidation of isoprene by OH (the dominant isoprene sink). When NO_x is sufficiently high, $ISOPO_2$ reacts mainly with NO to produce ozone (high-NO_x pathway). At lower NO_x levels, $ISOPO_2$ may instead react with HO_2 or other organic peroxy radicals, or isomerize, in which case ozone is not produced (low-NO_x pathways). Here we increase the molar yield of isoprene hydroperoxide (ISOPOOH) from the $ISOPO_2 + HO_2$ reaction to 93.7% based on observations of the minor channels of this reaction (Liu et al., 2013). Oxidation of ISOPOOH by OH produces isoprene epoxides (IEPOX) that subsequently react with OH or are taken up by aerosol (Paulot et al., 2009b; Marais et al., 2016). We use updated rates and products from Bates et al. (2014) for the reaction of IEPOX with OH.

$ISOPO_2$ isomerization produces hydroperoxyaldehydes (HPALDs) (Peeters et al., 2009; Crounse et al., 2011; Wolfe et al., 2012), and this is now explicitly included in the mechanism. HPALDs go on to react with OH or photolyze at roughly equal rates over the Southeast US. We use the HPALD+OH reaction rate constant from Wolfe et al. (2012) and the products of the reaction from Squire et al. (2015). The HPALD photolysis rate is calculated using the absorption cross-section of MACR, with a quantum yield of 1, as recommended by Peeters and Müller (2010). The photolysis products are taken from Stavrakou et al. (2010). We include a faster rate constant and revise the product yields for the self-reaction of $ISOPO_2$ according to Xie et al. (2013).

A number of studies have suggested that conversion of NO_2 to nitrous acid (HONO) by gas-phase or aerosol-phase pathways could provide a source of HO_x radicals following HONO photolysis (Li et al., 2014; Zhou et al., 2014). This mechanism would also provide a catalytic sink for ozone when NO_2 is produced by the NO + ozone reaction, viz.,

$$NO + O_3 \rightarrow NO_2 + O_2 \quad (1)$$

$$NO_2 \rightarrow HONO \text{ (by various pathways)} \quad (2)$$

$$HONO + h\upsilon \rightarrow NO + OH \quad (3)$$

Observations of HONO from the NOMADSS campaign (https://www2.acom.ucar.edu/campaigns/nomadss) indicate a mean daytime HONO concentration of 10 ppt in the Southeast US boundary layer (Zhou et al., 2014), whereas the standard gas-phase mechanism in GEOS-Chem version 9.02 yields less than 1 ppt. We added to the mechanism the pathway proposed by Li et al. (2014), in which HONO is produced by the reaction of the $HO_2 \bullet H_2O$ complex with NO_2, and reduced the corresponding rate constant to $k_{HO2 \bullet H2O+NO2} = 2 \times 10^{-12}$ cm^3 molecule^{-1} s^{-1} in order to obtain ~10 ppt daytime HONO in the Southeast US boundary layer. The resulting impact on boundary layer ozone concentrations is negligible.

2.2 Dry Deposition

The GEOS-Chem dry deposition scheme uses a resistance-in-series model based on Wesely (1989) as implemented by Wang et al. (1998). Underestimate of dry deposition has been invoked as a cause for model overestimates of ozone in the eastern

US (Lin et al., 2008; Walker, 2014). Daytime ozone deposition is determined principally by stomatal uptake. Here, we decrease the stomatal resistance from 200 s m^{-1} for both coniferous and deciduous forests (Wesely, 1989) by 20% to match summertime measurements of the ozone dry deposition velocity for a pine forest in North Carolina (Finkelstein et al., 2000) and for the Ozarks oak forest in southeast Missouri (Wolfe et al., 2015), both averaging 0.8 cm s^{-1} in the daytime. The mean ozone deposition velocity in GEOS-Chem along the SEAC^{4}RS boundary layer flight tracks in the Southeast US averages 0.7±0.3 cm s^{-1} for the daytime (9-16 local) surface layer. Deposition is suppressed in the model at night due to both stomatal closure and near-surface stratification, consistent with the Finkelstein et al. (2000) observations.

Deposition flux measurements for isoprene oxidation products at the Alabama SOAS site (http://soas2013.rutgers.edu) indicate higher deposition velocities than simulated by the standard GEOS-Chem model (Nguyen et al., 2015). As an expedient, Nguyen et al. (2015) scaled the Henry's law coefficients for these species in GEOS-Chem to match their observed deposition velocities and we follow their approach here. Other important depositing species include HNO_3 and peroxyacetyl nitrate (PAN), with mean deposition velocities along the SEAC^{4}RS Southeast US flight tracks in daytime of 3.9 cm s^{-1} and 0.6 cm s^{-1}, respectively.

2.3 Emissions

We use hourly US anthropogenic emissions from the 2011 EPA national emissions inventory (NEI11v1) at a horizontal resolution of 0.1° × 0.1° and adjusted to 2013 using national annual scaling factors (EPA, 2015). The scaling factor for NO_x emissions is 0.89. Further information on the use of the NEI11v1 in GEOS-Chem can be found here: http://wiki.seas.harvard.edu/geos-chem/index.php/EPA/NEI11_North_American_emissions/. The total national NO_x emission in NEI11v1 for 2013 is 3.5 Tg N. Initial implementation of this inventory in GEOS-Chem resulted in an overestimate of SEAC^{4}RS DC-8 observations of 60% for NO_x and 70% for HNO_3, and an overestimate of 71% for nitrate (NO_3^-) wet deposition fluxes measured by the National Acid Deposition Program (NADP) across the Southeast US. This suggests that NEI11v1 NO_x emissions are biased high. Errors in NO_x sources from soils, wildfire, or lightning cannot account for the overestimate because their magnitudes are small relative to fuel combustion, as shown below.

Emissions from power plant stacks, which represent 12% of the NEI11v1 NO_x emissions on an annual basis (EPA, 2015), are well constrained by continuous emission monitors. Other components of the NEI inventory are more uncertain. A number of studies have found that NEI emission estimates for mobile sources may be too high by a factor of two or more (Castellanos et al, 2011; Fujita et al., 2012; Brioude et al., 2013; Anderson et al., 2014). Lu et al. (2015) find good agreement between NEI emissions and top-down estimates from OMI NO_2, but they assume an error on NEI emissions of 50%.

Here we reduce NEI11v1 NO_x emissions (adjusted to 2013) by 60% (factor of 2.5) for all fuel combustion sources except power plants, amounting to a reduction of 53% (factor of 2.1) for total NEI11v1 emissions. There is no information in the

spatial pattern of bias that would warrant a more location-specific or source-specific reduction. The resulting US anthropogenic NO_x emissions from fuel combustion for 2013 total 1.7 Tg N a^{-1}. As shown in the next section, this reduction largely corrects the bias in the simulation of observations for NO_x and its oxidation products. Soil NO_x emissions, including emissions from fertilizer application, are computed according to Hudman et al. (2012), with a 50% reduction in the Midwest US based on a previous comparison with OMI NO_2 observations (Vinken et al., 2014). Open fire emissions are from the daily Quick Fire Emissions Database (QFED) (Darmenov and da Silva, 2014) with diurnal variability from the Western Regional Air Partnership (Air Sciences, 2005). We emit 40% of open fire NO_x emissions as PAN and 20% as HNO_3 to account for fast oxidation taking place in the fresh plume (Alvarado et al., 2010). Following Fischer et al. (2014), we inject 35% of fire emissions above the boundary layer, evenly between 3.5 and 5.5 km altitude.

We constrain the lightning NO_x source with satellite data as described by Murray et al. (2012). Lightning NO_x is mainly released at the top of convective updrafts following Ott et al. (2010). The standard GEOS-Chem model uses higher NO_x yields for mid-latitudes lightning (500 mol/flash) than for tropical (260 mol/flash) (Huntrieser et al., 2007, 2008; Hudman et al., 2007; Ott et al., 2010) with a fairly arbitrary boundary between the two at 23°N in North America and 35°N in Eurasia. Zhang et al. (2014) previously found that this leads GEOS-Chem to overestimate background ozone in the southwestern US and we find the same here for the eastern US and the Gulf of Mexico. We treat here all lightning in the 35°S-35°N band as tropical and thus remove the distinction between North America and Eurasia.

Figure 1 gives the resulting surface NO_x emissions for the Southeast US for August and September 2013. With the original NEI inventory, fuel combustion accounted for 81% of total surface NO_x emissions in the Southeast US (not including lightning). After reducing NEI emissions, the contribution from fuel combustion is still 68%.

Biogenic VOC emissions are from MEGAN v2.1, including isoprene, acetone, acetaldehyde, monoterpenes, and $>C_2$ alkenes. We reduce MEGAN v2.1 isoprene emissions by 15% to better match SEAC^{4}RS observations (Wolfe et al., 2015; Zhu et al., 2016). Yu et al. (2016) show the resulting isoprene emissions for the SEAC^{4}RS period.

3 Overestimate of NO_x emissions in the EPA NEI inventory

Figure 2 shows simulated and observed median vertical distributions of NO_x, total inorganic nitrate (gas-phase HNO_3+aerosol NO_3^-), and ozone concentrations along the SEAC^{4}RS flight tracks over the Southeast US. Here and elsewhere the data exclude urban plumes as diagnosed by $[NO_2] > 4$ ppb, open fire plumes as diagnosed by $[CH_3CN] > 200$ ppt, and stratospheric air as diagnosed by $[O_3]/[CO] > 1.25$ mol mol^{-1}. These filters exclude <1%, 7%, and 6% of the data respectively. We would not expect the model to be able to capture these features even at native resolution (Yu et al., 2016).

Model results in Figure 2 are shown both with the original NO_x emissions (dashed line) and with non-power plant NEI combustion emissions decreased by 60% (solid line). Decreasing emissions corrects the model bias for NO_x and also largely corrects the bias for inorganic nitrate. Boundary layer ozone is overestimated by 12 ppb with the original NO_x emissions but this bias disappears after decreasing the NO_x emissions.

Further support for decreasing NO_x emissions is offered by observed nitrate wet deposition fluxes from the NADP network (NADP, 2007). Figure 3 compares simulated and observed fluxes for the model with decreased NO_x emissions. Model values have been corrected for precipitation bias following the method of Paulot et al. (2014), in which the monthly deposition flux is assumed to scale to the 0.6^{th} power of the precipitation bias. We diagnose precipitation bias in the GEOS-5.11.0 data relative to high-resolution PRISM observations (http://prism.oregonstate.edu). For the Southeast US, the precipitation bias is -34% in August and -21% in September 2013.

We see from Figure 3 that the model with decreased NO_x emissions reproduces the spatial variability in the observations with minimal bias over the Southeast US domain shown in Figure 1 and across the rest of the country. In comparison, the model with original emissions had a 63% overestimate of the nitrate wet deposition flux nationally and a 71% overestimate in the Southeast. Thus the need to decrease NO_x emissions relative to NEI applies to the whole US, not just the Southeast. The high deposition fluxes along the Gulf of Mexico, both in the model and in the observations, reflect particularly large precipitation.

The model with decreased NO_x emissions also reproduces the spatial distribution of NO_x in the Southeast US boundary layer as observed in SEAC^{4}RS. This is shown in Figure 4 with simulated and observed concentrations of NO_x along the flight tracks below 1.5 km altitude. The spatial correlation coefficient is 0.71. There is no indication of regional patterns of model bias that would point to the need for a more selective adjustment of NO_x emissions.

4 Using satellite NO_2 data to verify NO_x emissions: sensitivity to upper troposphere

Observations of tropospheric NO_2 columns by solar backscatter from the OMI satellite instrument offer an additional constraint on NO_x emissions (Duncan et al., 2014; Lu et al., 2015). We compare the tropospheric columns simulated by GEOS-Chem with the NASA operational retrieval (Level 2, v2.1) (NASA, 2012; Bucsela et al., 2013) and the Berkeley High-Resolution (BEHR) retrieval (Russell et al., 2011). The NASA retrieval has been validated to agree with surface measurements to within ± 20% (Lamsal et al., 2014). Both retrievals fit the observed backscattered solar spectra to obtain a slant tropospheric NO_2 column, Ω_s, along the optical path of the backscattered radiation detected by the satellite. The slant column is converted to the vertical column, Ω_v, by using an air mass factor (*AMF*) that depends on the vertical profile of NO_2 and on the scattering properties of the surface and the atmosphere (Palmer et al., 2001):

$$\Omega_v = \frac{\Omega_S}{AMF} = \frac{\Omega_S}{\mathrm{AMF}_G \int_0^{z_T} w(z)S(z)dz} \quad (4)$$

In Equation 4, AMF_G is the geometric air mass factor that depends on the viewing geometry of the satellite, $w(z)$ is a scattering weight calculated by a radiative transfer model that describes the sensitivity of the backscattered radiation to NO_2 as a function of altitude, $S(z)$ is a shape factor describing the normalized vertical profile of NO_2 number density, and z_T is the tropopause. Scattering weights for NO_2 retrievals typically increase by a factor of 3 from the surface to the upper troposphere (Martin et al., 2002). Here we use our GEOS-Chem shape factors to re-calculate the AMFs in the NASA and BEHR retrievals as recommended by Lamsal et al. (2014) for comparing model and observations. We filter out cloudy scenes (cloud radiance fraction > 0.5) and bright surfaces (surface reflectivity > 0.3).

Figure 5 shows the mean NO_2 tropospheric columns from BEHR, NASA, and GEOS-Chem (with NO_x emission reductions applied) over the Southeast US for August-September 2013. The BEHR retrieval is on average 6% higher than the NASA retrieval. GEOS-Chem is on average 11±19% lower than the NASA retrieval and 16±18% lower than the BEHR retrieval. Without decreasing NEI NO_x emissions, GEOS-Chem would be biased high against both retrievals by 26-31%. The low bias in the model with reduced NO_x emissions does not appear to be caused by an overcorrection of surface emissions but rather by the upper troposphere. Figure 6 (top left panel) shows the mean vertical profile of NO_2 number density as measured from the aircraft by two independent instruments (NOAA and UC Berkeley) and simulated by GEOS-Chem. The observations show a secondary maximum in the upper troposphere above 10 km, absent in GEOS-Chem. It has been suggested that aircraft measurements of NO_2 in the upper troposphere could be biased high due to decomposition in the instrument inlet of thermally unstable NO_x reservoirs such as HNO_4 and methylperoxynitrate (Browne et al., 2011; Nault et al., 2015; Reed et al., 2016). This could possibly account for the difference between the NOAA and UC Berkeley measurements in the upper troposphere (Nault et al., 2015). At the surface, the median difference is 1.8×10^9 molecules cm^{-3} which is within the NOAA and UC Berkeley measurement uncertainties of +/- 0.030 ppbv + 7% and +/- 5%, respectively.

The top right panel of Figure 6 shows the cumulative contributions from different altitudes to the slant NO_2 column measured by the satellite, using the median vertical profiles from the left panel and applying mean altitude-dependent scattering weights from the NASA and BEHR retrievals. The boundary layer below 1.5 km contributes only 19-28% of the column. The upper troposphere above 8 km contributes 32-49% in the aircraft observations and 23% in GEOS-Chem. Much of the observed upper tropospheric NO_2 likely originates from lightning and is broadly distributed across the Southeast because of the long lifetime of NO_x at that altitude (Li et al., 2005; Bertram et al., 2007; Hudman et al., 2007). The NO_2 vertical profile (shape factor) assumed in the BEHR retrieval does not include any lightning influence, and the Global Modeling Initiative (GMI) model vertical profile assumed in the NASA retrieval likely underestimates the upper tropospheric NO_2 similarly to GEOS-Chem in Figure 6. These underestimates of upper tropospheric NO_2 in the retrieval

shape factors will cause a negative bias in the AMF and therefore a positive bias in the retrieved vertical columns. This could explain the lower GEOS-Chem column in Figure 5 as compared to the retrievals.

The GEOS-Chem underestimate of observed upper tropospheric NO_2 in Figure 6 is partially driven by NO/NO_2 partitioning. The bottom left panel of Figure 6 shows the $[NO]/[NO_2]$ concentration ratio in GEOS-Chem and in the observations (NOAA for NO, UC Berkeley for NO_2). One would expect the $[NO]/[NO_2]$ concentration ratio in the daytime upper troposphere to be controlled by photochemical steady-state:

$$NO + O_3 \rightarrow NO_2 + O_2 \quad (5)$$

$$NO + HO_2/RO_2 \rightarrow NO_2 + OH/RO \quad (6)$$

$$NO_2 + h\nu \xrightarrow{O_2} NO + O_3 \quad (7)$$

with reaction (6) playing only a minor role so that $[NO]/[NO_2] \approx k_7/(k_5[O_3])$, defining the $NO\text{-}NO_2\text{-}O_3$ photochemical steady state (PSS). The PSS plotted in Figure 6 agrees closely with GEOS-Chem, with the relatively small differences due to reaction (6). Such agreement has previously been found when comparing photochemical models with observed $[NO]/[NO_2]$ ratios from aircraft in the marine upper troposphere (Schultz et al., 1999) and lower stratosphere (Del Negro et al., 1999). The SEAC^{4}RS observations show large departure.

Zhu et al. (2016) found that GEOS-Chem underestimates the observed HCHO concentrations in the upper troposphere during SEAC^{4}RS by a factor of 3, implying that the model underestimates the HO_x source from convective injection of HCHO and peroxides (Prather and Jacob, 1997; Müller and Brasseur, 1999). HO_2 observations over the central US in summer during the SUCCESS aircraft campaign suggest that this convective injection increases HO_x concentrations in the upper troposphere by a factor of 2 (Jaeglé et al., 1998). The bottom right panel of Figure 6 shows median modeled and observed vertical profiles of the HO_x reservoir hydrogen peroxide (H_2O_2) during SEAC^{4}RS over the Southeast US. GEOS-Chem underestimates observed H_2O_2 by a mean factor of 1.7 above 8km. The middle right panel of Figure 6 shows the predicted $[NO]/[NO_2]$ ratio if modeled convective injection of HO_2 and RO_2 precursors is underestimated by a factor of 2. While such an underestimate is insufficient to reconcile simulated and observed $[NO]/[NO_2]$ concentration ratios, the contribution to the $[NO]/[NO_2]$ ratio from Reaction 6 would be much more significant than previously estimated.

The PSS and GEOS-Chem simulation of the NO/NO_2 concentration ratio in Figure 6 use $k_5 = 3.0\times10^{-12}\exp[-1500/T]$ cm^3 molecule^{-1} s^{-1} and spectroscopic information for k_7 from Sander et al. (2011). The NO_2 photolysis frequencies k_7 computed locally by GEOS-Chem are on average within 10% of the values determined in SEAC^{4}RS from measured actinic fluxes (Shetter and Muller, 1999). It is possible that the strong thermal dependence of k_5 has some error, considering that only one direct measurement has been published for the cold temperatures of the upper troposphere (Borders and Birks, 1982). Cohen et al. (2000) found that reducing the activation energy of k_5 by 15% improved model agreement in the lower stratosphere.

Correcting the discrepancy between simulated and observed [NO]/[NO_2] ratios in the upper troposphere in Figure 6 would require a similar reduction to the activation energy of k_5, but this reduction would negatively impact the surface comparison. This inconsistency of the observed [NO]/[NO_2] ratio with basic theory needs to be resolved, as it affects the inference of NO_x emissions from satellite NO_2 column measurements. Notwithstanding this inconsistency, we find that NO_2 in the upper troposphere makes a significant contribution to the tropospheric NO_2 column observed from space.

5 Isoprene oxidation pathways

Measurements aboard the SEAC^{4}RS aircraft included first-generation isoprene nitrates (ISOPN), isoprene hydroperoxide (ISOPOOH), and hydroperoxyaldehydes (HPALDs) (Crounse et al., 2006; Paulot et al., 2009a; St. Clair et al., 2010; Crounse et al., 2011; Beaver et al., 2012; Nguyen et al., 2015). The measurement uncertainties are large (30%, 40%, and 50%, respectively (Nguyen et al., 2015)). These are unique products of the $ISOPO_2$ + NO, $ISOPO_2$ + HO_2, and $ISOPO_2$ isomerization pathways and thus track whether oxidation of isoprene proceeds by the high-NO_x pathway (producing ozone) or the low-NO_x pathways. Figure 2 (bottom row) compares simulated and observed concentrations. All three gases are restricted to the boundary layer because of their short lifetimes. Mean model concentrations in the lowest altitude bin (Figure 2, approximately 400m above ground) differ from observations by 19% for ISOPN and -50% for HPALDs. The GEOS-Chem simulation of organic nitrates including ISOPN is further discussed in Fisher et al. (2016).

The bias for HPALDs is within the uncertainty of the kinetics and measurement. Our HPALD source is based on the $ISOPO_2$ isomerization rate constant from Crounse et al. (2011). A theoretical calculation by Peeters et al. (2014) suggests a rate constant that is 1.8× higher, which would reduce the model bias for HPALDs and ISOPOOH and increase boundary layer OH by 8%. GEOS-Chem overestimates ISOPOOH by 74% below 1.5 km. Recent work by St. Clair et al. (2015) found that the reaction rate of ISOPOOH + OH to form IEPOX is approximately 10% faster than the rate given by Paulot et al. (2009b), which would further reduce the model overestimate. It is likely that after these changes the GEOS-Chem overestimate of ISOPOOH would be within measurement uncertainty. For both ISOPOOH and HPALDs, GEOS-Chem captures much of the spatial variability (r = 0.8 and 0.7, respectively).

Figure 7 shows the model branching ratios for the fate of the $ISOPO_2$ radical by tracking the mass of $ISOPO_2$ reacting via the high-NO_x pathway ($ISOPO_2$+NO) and the low-NO_x pathways over the Southeast US domain. The mean branching ratios for the Southeast US are $ISOPO_2$+NO 54%, $ISOPO_2$+HO_2 26%, $ISOPO_2$ isomerization 15%, and $ISOPO_2$+RO_2 5%. The lack of dominance of the high-NO_x pathway is due in part to the spatial segregation of isoprene and NO_x emissions (Yu et al., 2016). This segregation also buffers the effect of changing NO_x emissions on the fate of isoprene. Our original simulation with higher total NO_x emissions (unadjusted NEI11v1) had a branching ratio for the $ISOPO_2$+NO reaction of 62%, as compared to 54% in our standard simulation.

6 Implications for ozone: aircraft and ozonesonde observations

Figure 2 compares simulated and observed median vertical profiles of ozone concentrations over the Southeast US during SEAC^{4}RS. There is no significant bias through the depth of the tropospheric column. The median ozone concentration below 1.5 km is 49 ppb in the observations and 51 ppb in the model. We also find excellent model agreement across the US with the SEACIONS ozonesonde network (Figure 8). The successful simulation of ozone is contingent on the decrease in NO_x emissions relative to the NEI inventory. As shown in Figure 2, a simulation with the unadjusted NEI emissions overestimates boundary layer ozone by 12 ppb.

The model also has some success in reproducing the spatial variability of boundary layer ozone seen from the aircraft, as shown in Figure 4. The correlation coefficient is $r = 0.71$ on the 0.25°×0.3125° model grid, and patterns of high and low ozone concentration are consistent. The highest observed ozone (>75 ppb) was found in air influenced by agricultural burning along the Mississippi River and by outflow from Houston over Louisiana. GEOS-Chem does not capture the extreme values and this probably reflects a dilution effect (Yu et al., 2016).

A critical parameter for understanding ozone production is the ozone production efficiency (OPE) (Liu et al., 1987), defined as the number of ozone molecules produced per molecule of NO_x emitted. This can be estimated from atmospheric observations by the relationship between odd oxygen ($O_x \equiv O_3+NO_2$) and the sum of products of NO_x oxidation, collectively called NO_z and including inorganic and organic nitrates (Trainer et al., 1993; Zaveri, 2003). The O_x vs. NO_z linear relationship (as derived from a linear regression) provides an upper estimate of the OPE because of rapid deposition of NO_y, mainly HNO_3 (Trainer et al., 2000; Rickard et al., 2002).

Figure 9 shows the observed and simulated daytime (9-16 local) O_x vs. NO_z relationship in the SEAC^{4}RS data below 1.5 km, where NO_z is derived from the observations as NO_y-$NO_x \equiv HNO_3$ + aerosol nitrate + PAN + alkyl nitrates. The resulting OPE from the observations (17.4±0.4 mol mol^{-1}) agrees well with GEOS-Chem (16.7±0.3). Previous work during the INTEX-NA aircraft campaign in summer 2004 found an OPE of 8 below 4 km (Mena-Carrasco et al., 2007). By selecting INTEX-NA data only for the Southeast and below 1.5 km we find an OPE of 14.1±1.1 (Figure 9, right panel). The median NO_z was 1.1 ppb during SEAC^{4}RS and 1.5 ppb during INTEX-NA, a decrease of approximately 40%. With the original NEI11v1 NO_x emissions (53% higher), the OPE from GEOS-Chem would be 14.7±0.3. Both the INTEX-NA data and the model are consistent with the expectation that OPE increases with decreasing NO_x emissions (Liu et al., 1987).

7 Implications for ozone: surface air

Figure 10 compares maximum daily 8-h average (MDA8) ozone values at the US EPA Clean Air Status and Trends Network (CASTNET) sites in June-August 2013 to the corresponding GEOS-Chem values. The model has a mean positive bias of 6±14 ppb with no significant spatial pattern. The model is unable to match the low tail in the observations, including a significant population with MDA8 ozone less than 20 ppb.

The positive bias in the model for surface ozone is remarkable considering that the model is unbiased relative to aircraft observations below 1.5 km altitude (Figures 2 and 4). A standard explanation for model overestimates of surface ozone over the Southeast US, first proposed by Fiore et al. (2003) and echoed in the review by McDonald-Buller et al. (2011), is excessive ozone over the Gulf of Mexico, which is the prevailing low-altitude inflow. We find that this is not the case. SEAC^{4}RS included four flights over the Gulf of Mexico, and Figure 11 compares simulated and observed vertical profiles of ozone and NO_x concentrations that show no systematic bias. The median ozone concentration in the marine boundary layer is 26 ppb in the observations and 29 ppb in the model. This successful simulation is due to our adjustment of lightning NO_x emission (Section 2.3); a sensitivity test with the original (twice higher) GEOS-Chem lightning emissions in the southern US increases surface ozone over the Gulf of Mexico by up to 6 ppb. The aircraft observations in Figure 4 show no indication of a coastal depletion that might be associated with halogen chemistry. Remarkably, the median ozone over the Gulf of Mexico is higher than approximately 8% of MDA8 values at sites in the Southeast.

It appears instead that there is a model bias in boundary layer vertical mixing and chemical production. Figure 12 shows the median ozonesonde profile at a higher vertical resolution over the Southeast US (Huntsville, Alabama and St. Louis, Missouri sites) during SEAC^{4}RS as compared to GEOS-Chem below 1.5 km. The ozonesondes indicate a decrease of 7 ppb from 1.5 km to the surface, whereas GEOS-Chem features a reverse gradient of increasing ozone from 1.5 to 1 km with flat concentrations below. Preliminary inspection suggests that this may reflect excessively dry conditions in the GEOS-5.11.0 meteorological fields, promoting boundary layer production and vertical mixing of ozone. Such a bias might not be detected in the aircraft data, collected mainly under fair weather conditions.

8 Conclusions

We used aircraft (SEAC^{4}RS), surface, satellite, and ozonesonde observations from August and September 2013, interpreted with the GEOS-Chem chemical transport model, to better understand the factors controlling surface ozone in the Southeast US. Models tend to overestimate ozone in that region. Determining the reasons behind this overestimate is critical to the design of efficient emission control strategies to meet the ozone NAAQS.

A major finding from this work is that the EPA National Emission Inventory (NEI11v1) for NO_x (the limiting precursor for ozone formation) is biased high across the US by as much as a factor of 2. Evidence for this comes from (1) SEAC^{4}RS observations of NO_x and its oxidation products, (2) NADP network observations of nitrate wet deposition fluxes, and (3) OMI satellite observations of NO_2. Presuming no error in emissions from large power plants with continuous emission monitors (12% of unadjusted NEI inventory), we suggest that emissions from other industrial sources and mobile sources must be decreased by a factor of 2.5 from NEI values. We estimate that anthropogenic NO_x emissions in the US in 2013 were 1.7 Tg N a^{-1}.

OMI NO_2 satellite data over the Southeast US are consistent with this downward correction of NO_x emissions but interpretation is complicated by the large contribution of the free troposphere to the NO_2 tropospheric column retrieved from the satellite. Observed (aircraft) and simulated vertical profiles indicate that NO_2 below 2 km contributes only 20-35% of the tropospheric column detected from space while NO_2 above 8 km (mainly from lightning) contributes 25-50%. Current retrievals of satellite NO_2 data do not properly account for this elevated pool of upper tropospheric NO_2, so that the reported tropospheric NO_2 columns are biased high. More work is needed on the chemistry maintaining high levels of NO_2 in the upper troposphere.

Isoprene emitted by vegetation is the main VOC precursor of ozone in the Southeast in summer, but we find that only 50% reacts by the high-NO_x pathway to produce ozone. This is consistent with detailed aircraft observations of isoprene oxidation products from the aircraft. The high-NO_x fraction is only weakly sensitive to the magnitude of NO_x emissions because isoprene and NO_x emissions are spatially segregated. The ability to properly describe high- and low-NO_x pathways for isoprene oxidation is critical for simulating ozone and it appears that the GEOS-Chem mechanism is successful for this purpose.

Our updated GEOS-Chem simulation with decreased NO_x emissions provides an unbiased simulation of boundary layer and free tropospheric ozone measured from aircraft and ozonesondes during SEAC^{4}RS. Decreasing NO_x emissions is critical to this success as the original model with NEI emissions overestimated boundary layer ozone by 12 ppb. The ozone production efficiency (OPE) inferred from O_x vs. NO_z aircraft correlations in the mixed layer is also well reproduced. Comparison to the INTEX-NA aircraft observations over the Southeast in summer 2004 indicates a 14% increase in OPE associated with a 40% reduction in NO_x emissions.

Despite the unbiased simulation of boundary layer ozone, GEOS-Chem overestimates MDA8 surface ozone observations in the Southeast US in summer by 6±14 ppb. Daytime ozonesonde data indicate a 7 ppb decrease from 1.5 km to the surface that GEOS-Chem does not capture. This may be due to excessively dry conditions in the GEOS meteorological data used to drive GEOS-Chem, resulting in excessive boundary layer ozone production and mixing. Such a bias may not be detected in

the aircraft data, generally collected under fair-weather conditions. Investigating this source of bias and its prevalence across models will be the topic of a follow-up paper.

Acknowledgements

We are grateful to the entire NASA SEAC^{4}RS team for their help in the field. We thank Tom Ryerson for his measurements of NO and NO_2 from the NOAA NO_yO_3 instrument. We thank L. Gregory Huey for the use of his CIMS PAN measurements. We thank Fabien Paulot and Jingqiu Mao for their helpful discussions of isoprene chemistry. We thank Christoph Keller for his help in implementing the NEI11v1 emissions into GEOS-Chem. We acknowledge the EPA for providing the 2011 North American emission inventory, and in particular George Pouliot for his help and advice. These emission inventories are intended for research purposes. A technical report describing the 2011-modeling platform can be found at: http://www.epa.gov/ttn/chief/net/2011nei/2011_nei_tsdv1_draft2_june2014.pdf. A description of the 2011 NEI can be found at: http://www.epa.gov/ttnchie1/net/2011inventory.html. This work was supported by the NASA Earth Science Division and by STAR Fellowship Assistance Agreement no. 91761601-0 awarded by the US Environmental Protection Agency (EPA). It has not been formally reviewed by EPA. The views expressed in this publication are solely those of the authors. JAF acknowledges support from a University of Wollongong Vice Chancellor's Postdoctoral Fellowship. This research was undertaken with the assistance of resources provided at the NCI National Facility systems at the Australian National University through the National Computational Merit Allocation Scheme supported by the Australian Government.

References

Air Sciences, I.: 2002 Fire Emission Inventory for the WRAP Region - Phase II, Western Governors Association/Western Regional Air Parnership, 2005.

Alvarado, M. J., Logan, J. A., Mao, J., Apel, E., Riemer, D., Blake, D., Cohen, R. C., Min, K. E., Perring, A. E., Browne, E. C., Wooldridge, P. J., Diskin, G. S., Sachse, G. W., Fuelberg, H., Sessions, W. R., Harrigan, D. L., Huey, G., Liao, J., Case-Hanks, A., Jimenez, J. L., Cubison, M. J., Vay, S. A., Weinheimer, A. J., Knapp, D. J., Montzka, D. D., Flocke, F. M., Pollack, I. B., Wennberg, P. O., Kurten, A., Crounse, J., Clair, J. M. S., Wisthaler, A., Mikoviny, T., Yantosca, R. M., Carouge, C. C., and Le Sager, P.: Nitrogen oxides and PAN in plumes from boreal fires during ARCTAS-B and their impact on ozone: an integrated analysis of aircraft and satellite observations, Atmos. Chem. Phys., 10, 9739-9760, doi:10.5194/acp-10-9739-2010, 2010.

Anderson, D. C., Loughner, C. P., Diskin, G., Weinheimer, A., Canty, T., P., Salawitch, R. J., Worden, H. M., Fried, A., Mikoviny, T., Wisthaler, A., and Dickerson, R., R.: Measured and modeled CO and NOy in DISCOVER-AQ: An evaluation of emissions and chemistry over the eastern US, Atmos. Environ., 96, 78-87, doi:10.1016/j.atmosenv.2014.07.004, 2014.

Bates, K. H., Crounse, J. D., St Clair, J. M., Bennett, N. B., Nguyen, T. B., Seinfeld, J. H., Stoltz, B. M., and Wennberg, P. O.: Gas Phase Production and Loss of Isoprene Epoxydiols, J. Phys. Chem.-US A, 118, 1237-1246, doi: 10.1021/Jp4107958, 2014.

Beaver, M. R., St. Clair, J. M., Paulot, F., Spencer, K. M., Crounse, J. D., LaFranchi, B. W., Min, K. E., Pusede, S. E., Woolridge, P. J., Schade, G. W., Park, C., Cohen, R. C., and Wennberg, P. O.: Importance of biogenic precursors to the budget of organic nitrates: observations of multifunctional organic nitrates by CIMS and TD-LIF during BEARPEX 2009, Atmos. Chem. Phys., 12, 5773-5785, 2012.

Bertram, T. H., Perring, A. E., Wooldridge, P. J., Crounse, J. D., Kwan, A. J., Wennberg, P. O., Scheuer, E., Dibb, J., Avery, M., Sachse, G., Vay, S. A., Crawford, J. H., McNaughton, C. S., Clarke, A., Pickering, K. E., Fuelberg, H., Huey, G., Blake, D. R., Singh, H. B., Hall, S. R., Shetter, R. E., Fried, A., Heikes, B. G., and Cohen, R. C.: Direct Measurements of the Convective Recycling of the Upper Troposphere, Science, 315, doi:10.1126/science.1134548, 2007.

Bey, I., Jacob, D. J., Yantosca, R. M., Logan, J. A., Field, B. D., Fiore, A. M., Li, Q. B., Liu, H. G. Y., Mickley, L. J., and Schultz, M. G.: Global modeling of tropospheric chemistry with assimilated meteorology: Model description and evaluation, J. Geophys. Res.-Atmos, 106, 23073-23095, doi:10.1029/2001jd000807, 2001.

Borders, R. A., and Birks, J. W.: High-Precision Measurements of Activation Energies over Small Temperature Intervals: Curvature in the Arrhenius Plot for the Reaction NO + O_3 --> NO_2 + O_2, J. Phys. Chem.-US, 86, 3295-3302, 1982.

Brioude, J., Angevine, W. M., Ahmadov, R., Kim, S. W., Evan, S., McKeen, S. A., Hsie, E. Y., Frost, G. J., Neuman, J. A., Pollack, I. B., Peischl, J., Ryerson, T. B., Holloway, J., Brown, S. S., Nowak, J. B., Roberts, J. M., Wofsy, S. C., Santoni, G. W., Oda, T., and Trainer, M.: Top-down estimate of surface flux in the Los Angeles Basin using a mesoscale inverse modeling technique: assessing anthropogenic emissions of CO, NO_x and CO_2 and their impacts, Atmos. Chem. Phys., 13, 3661-3677, doi:10.5194/acp-13-3661-2013, 2013.

Brown-Steiner, B., Hess, P. G., and Lin, M. Y.: On the capabilities and limitations of GCCM simulations of summertime regional air quality: A diagnostic analysis of ozone and temperature simulations in the US using CESM CAM-Chem, Atmos. Environ., 101, 134-148, doi:10.1016/j.atmosenv.2014.11.001, 2015.

Browne, E. C., Perring, A. E., Wooldridge, P. J., Apel, E., Hall, S. R., Huey, L. G., Mao, J., Spencer, K. M., Clair, J. M. S., Weinheimer, A. J., Wisthaler, A., and Cohen, R. C.: Global and regional effects of the photochemistry of $CH_3O_2NO_2$: evidence from ARCTAS, Atmos. Chem. Phys., 11, 4209-4219, doi:10.5194/acp-11-4209-2011, 2011.

Brunner, D., Staehelin, J., Jeker, D., Wernli, H., and Schumann, U.: Nitrogen oxides and ozone in the tropopause region of the Northern Hemisphere: Measurements from commercial aircraft in 1996/1996 and 1997, J. Geophys. Res., 106, 27,673-627,699, 2001.

Bucsela, E. J., Krotkov, N. A., Celarier, E. A., Lamsal, L. N., Swartz, W. H., Bhartia, P. K., Boersma, K. F., Veefkind, J. P., Gleason, J. F., and Pickering, K. E.: A new stratospheric and tropospheric NO_2 retrieval algorithm for nadir-viewing

satellite instruments: applications to OMI, Atmospheric Measurement Techniques, 6, 2607-2626, doi:10.5194/amt-6-2607-2013, 2013.

Canty, T. P., Hembeck, L., Vinciguerra, T. P., Anderson, D. C., Goldberg, D. L., Carpenter, S. F., Allen, D. J., Loughner, C. P., Salawitch, R. J., and Dickerson, R. R.: Ozone and NO_x chemistry in the eastern US: evaluation of CMAQ/CB05 with satellite (OMI) data, Atmos. Chem. Phys., 15, 10965–10982, doi:10.5194/acp-15-10965-2015, 2015.

Carpenter, L. J., Clemitshaw, K. C., Burgess, R. A., Penkett, S. A., Cape, J. N., and McFadyen, G. G.: Investigation and evaluation of the NO_x/O_3 photochemical steady state, Atmos. Environ., 32, 3353-3365, 1998.

Castellanos, P. Marufu, L. T., Doddridge, B. G., Taubman, B. F., Schwab, J. J., Hains, J. C., Ehrman, S. H., Dickerson, R. R.: Ozone, oxides of nitrogen, and carbon monoxide during pollution events over the eastern United States: An evaluation of emissions and vertical mixing, J. Geophys. Res., 116, D16307, doi:10.1029/2010JD014540, 2011.

Chen, D., Wang, Y. X., McElroy, M. B., He, K., Yantosca, R. M., and Le Sager, P.: Regional CO pollution in China simulated by the high-resolution nested-grid GEOS-Chem model, Atmos. Chem. Phys., 9, 3825-3839, 2009.

Cohen, R. C., Perkins, K. K., Koch, L. C., Stimpfle, R. M., Wennberg, P. O., Hanisco, T. F., Lanzendorf, E. J., Bonne, G. P., Voss, P. B., Salawitch, R. J., Del Negro, L. A., Wilson, J. C., McElroy, C. T., and Bui, T. P.: Quantitative constraints on the atmospheric chemistry of nitrogen oxides: An analysis along chemical coordinates, J. Geophys. Res., 105, 24,283-224,304, 2000.

Crounse, J. D., McKinney, K. A., Kwan, A. J., and Wennberg, P. O.: Measurement of gas-phase hydroperoxides by chemical ionization mass spectrometry (CIMS), Anal. Chem., 78, 6726-6732, 2006.

Crounse, J. D., Paulot, F., Kjaergaard, H. G., and Wennberg, P. O.: Peroxy radical isomerization in the oxidation of isoprene, Phys. Chem. Chem. Phys., 13, 13607-13613, doi:10.1039/c1cp21330j, 2011.

Darmenov, A. S., and da Silva, A.: The Quick Fire Emissions Dataset (QFED) Documentatino of versions 2.1, 2.2 and 2.4, NASA, 2014.

Dibb, J. E., Talbot, R. W., Scheuer, E. M., Seid, G., Avery, M., A., and Singh, H. B.: Aerosol chemical composition in Asian continental outflow during the TRACE-P campaign: Comparison with PEM-West B, J. Geophys. Res., 108, doi:10.1029/2002jd003111, 2003.

Del Negro, L. A., Fahey, D. W., Gao, R. S., Donnelly, S. G., Keim, E. R., Neuman, J. A., Cohen, R. C., Perkins, K. K., Koch, L. C., Salawitch, R. J., Lloyd, S. A., Proffitt, M. H., Margitan, J. J., Stimpfle, R. M., Bonne, G. P., Voss, P. B., Wennberg, P. O., McElroy, C. T., Swartz, W. H., Kusterer, T. L., Anderson, D. E., Lait, L. R., and Bui, T. P.: Comparison of modeled and observed values of NO_2 and JNO_2 during the Photochemistry of Ozone Loss in the Arctic Region in Summer (POLARIS) mission, J. Geophys. Res., 104, 26687, doi:10.1029/1999jd900246, 1999.

Duncan, B. N., Prados, A. I., Lamsal, L. N., Liu, Y., Streets, D. G., Gupta, P., Hilsenrath, E., Kahn, R. A., Nielsen, J. E., Beyersdorf, A. J., Burton, S. P., Fiore, A. M., Fishman, J., Henze, D. K., Hostetler, C. A., Krotkov, N. A., Lee, P., Lin, M., Pawson, S., Pfister, G., Pickering, K. E., Pierce, R. B., Yoshida, Y., and Ziemba, L. D.: Satellite data of atmospheric pollution for U.S. air quality applications: Examples of applications, summary of data end-user

resources, answers to FAQs, and common mistakes to avoid, Atmos. Environ., 94, 647-662, doi:10.1016/j.atmosenv.2014.05.061, 2014.

EPA: Integrated Science Assessment for Ozone and Related Photochemical Oxidatns, U.S. Environmental Protection Agency, Research Triangle Park, NC, 2013.

National Emissions Inventory (NEI) Air Pollutant Emission Trends Data: http://www.epa.gov/ttn/chief/trends/index.html, 2015.

Finkelstein, P. L., Ellestad, T. G., Clarke, J. F., Meyers, T. P., Schwede, D. B., Hebert, E. O., and Neal, J. A.: Ozone and sulfur dioxide dry deposition to forests: Observations and model evaluation, J. Geophys. Res.-Atmos, 105, 15365-15377, doi:10.1029/2000jd900185, 2000.

Fiore, A. M., Jacob, D. J., Liu, H., Yantosca, R. M., Fairlie, T. D., and Li, Q.: Variability in surface ozone background over the United States: Implications for air quality policy, J. Geophys. Res.-Atmos, 108, doi:10.1029/2003jd003855, 2003.

Fiore, A. M., Horowitz, L. W., Purves, D. W., Levy, H., Evans, M. J., Wang, Y., Li, Q., and Yantosca, R.: Evaluating the contribution of changes in isoprene emissions to surface ozone trends over the eastern United States, J. Geophys. Res., 110, doi:10.1029/2004jd005485, 2005.

Fiore, A. M., Dentener, F. J., Wild, O., Cuvelier, C., Schultz, M. G., Hess, P., Textor, C., Schulz, M., Doherty, R. M., Horowitz, L. W., MacKenzie, I. A., Sanderson, M. G., Shindell, D. T., Stevenson, D. S., Szopa, S., Van Dingenen, R., Zeng, G., Atherton, C., Bergmann, D., Bey, I., Carmichael, G., Collins, W. J., Duncan, B. N., Faluvegi, G., Folberth, G., Gauss, M., Gong, S., Hauglustaine, D., Holloway, T., Isaksen, I. S. A., Jacob, D. J., Jonson, J. E., Kaminski, J. W., Keating, T. J., Lupu, A., Marmer, E., Montanaro, V., Park, R. J., Pitari, G., Pringle, K. J., Pyle, J. A., Schroeder, S., Vivanco, M. G., Wind, P., Wojcik, G., Wu, S., and Zuber, A.: Multimodel estimates of intercontinental source-receptor relationships for ozone pollution, J. Geophys. Res., 114, doi:10.1029/2008jd010816, 2009.

Fischer, E. V., Jacob, D. J., Yantosca, R. M., Sulprizio, M. P., Millet, D. B., Mao, J., Paulot, F., Singh, H. B., Roiger, A., Ries, L., Talbot, R. W., Dzepina, K., and Deolal, S. P.: Atmospheric peroxyacetyl nitrate (PAN): a global budget and source attribution, Atmos. Chem. Phys., 14, 2679-2698, 2014.

Fisher, J. A., Jacob, D. D., Travis, K. R., Kim, P. S., Marais, E., Miller, C. C., Yu, K., Zhu, L., Yantosca, R. M., Sulprizio, M. P., Mao, J., Wennberg, P. O., Crounse, J. D., Teng, A. P., Nguyen, T. B., St Clair, J. M., Romer, P., Nault, B. A., Wooldridge, P. J., Jimenez, J. L., Campuzano-Jost, P., Day, D. A., Shepson, P. B., Xiong, F., Blake, D. R., Goldstein, A. H., Misztal, P. K., Hanisco, T. F., Wolfe, G. M., Ryerson, T. B., Wisthaler, A., and Mikoviny, T.: Organic nitrate chemistry and its implications for nitrogen budgets in an isoprene- and monoterpene-rich atmosphere: constrains from aircraft (SEAC4RS) and ground-based (SOAS) observations in the Southeast US, Atmos. Chem. Phys., 6, 5969-5991, doi:10.5194/acp-16-5969-2016 , 2016.

Fujita, E. M., Campbell, D. E., Zielinska, B., Chow, J. C., Lindhjem, C. E., DenBleyker, A., Bishop, G. A., Schuchmann, B. G., Stedman, D. H., and Lawson, D. R.: Comparison of the MOVES2010a, MOBILE6.2, and EMFAC2007 mobile source emission models with on-road traffic tunnel and remote sensing measurements, J. Air Waste Manage., 62, 1134-1149, doi:10.1080/10962247.2012.699016, 2012.

Holtslag, A., and Boville, B.: Local versus nonlocal boundary-layer diffusion in a global climate model, J. Climate, 6, 1825, 1993.

Horowitz, L. W., Fiore, A. M., Milly, G. P., Cohen, R. C., Perring, A., Wooldridge, P. J., Hess, P. G., Emmons, L. K., and Lamarque, J. F.: Observational constraints on the chemistry of isoprene nitrates over the eastern United States, J. Geophys. Res.-Atmos, 112, doi:0.1029/2006jd007747, 2007.

Hudman, R. C., Jacob, D. J., Turquety, S., Leibensperger, E. M., Murray, L. T., Wu, S., Gilliland, A. B., Avery, M., Bertram, T. H., Brune, W., Cohen, R. C., Dibb, J. E., Flocke, F. M., Fried, A., Holloway, J., Neuman, J. A., Orville, R., Perring, A., Ren, X., Sachse, G. W., Singh, H. B., Swanson, A., and Wooldridge, P. J.: Surface and lightning sources of nitrogen oxides over the United States: Magnitudes, chemical evolution, and outflow, J. Geophys. Res., 112, doi:10.1029/2006jd007912, 2007.

Hudman, R. C., Moore, N. E., Mebust, A. K., Martin, R. V., Russell, A. R., Valin, L. C., and Cohen, R. C.: Steps towards a mechanistic model of global soil nitric oxide emissions: implementation and space based-constraints, Atmos. Chem. Phys., 12, 7779-7795, doi:10.5194/acp-12-7779-2012, 2012.

Huntrieser, H., Schlager, H., Roiger, A., Lichtenstern, M., Schu- mann, U., Kurz, C., Brunner, D., Schwierz, C., Richter, A., and Stohl, A.: Lightning-produced NOx over Brazil during TROC- CINOX: airborne measurements in tropical and subtropical thun- derstorms and the importance of mesoscale convective systems, Atmos. Chem. Phys., 7, 2987–3013, doi:10.5194/acp-7-2987-2007, 2007.

Huntrieser, H., Schumann, U., Schlager, H., Höller, H., Giez, A., Betz, H.-D., Brunner, D., Forster, C., Pinto Jr., O., and Calheiros, R.: Lightning activity in Brazilian thunderstorms during TROCCINOX: implications for NOx production, Atmos. Chem. Phys., 8, 921–953, doi:10.5194/acp-8-921-2008, 2008.

Jacobs, M. I., Burke, W. J., and Elrod, M. J.: Kinetics of the reactions of isoprene-derived hydroxynitrates: gas phase epoxide formation and solution phase hydrolysis, Atmos. Chem. Phys., 14, 8933-8946, doi:10.5194/acp-14-8933-2014, 2014.

Jaeglé, L. Jacob, D. J., Wang, Y., Weinheimer, A. J. Ridley, B. A., Campos, T. L., Sachse, G. W., Hagen, D. E.: Sources and chemistry of NO_x in the upper troposphere over the United States, Geophys. Res. Lett. 25(10), 1705-1708, 1998.

Kim, P. S., Jacob, D. J., Fisher, J. A., Travis, K., Yu, K., Zhu, L., Yantosca, R. M., Sulprizio, M. P., Jimenez, J. L., Campuzano-Jost, P., Froyd, K. D., Liao, J., Hair, J. W., Fenn, M. A., Butler, C. F., Wagner, N. L., Gordon, T. D., Welti, A., Wennberg, P. O., Crounse, J. D., St. Clair, J. M., Teng, A. P., Millet, D. B., Schwarz, J. P., Markovic, M. Z., and Perring, A. E.: Sources, seasonality, and trends of Southeast US aerosol: an integrated analysis of surface,

aircraft, and satellite observations with the GEOS-Chem chemical transport model, Atmos. Chem. Phys., 15, 10411-10433, doi:10.5194/acp-15-10411-2015, 2015.

Lamsal, L. N., Krotkov, N. A., Celarier, E. A., Swartz, W. H., Pickering, K. E., Bucsela, E. J., Gleason, J. F., Martin, R. V., Philip, S., Irie, H., Cede, A., Herman, J., Weinheimer, A., Szykman, J. J., and Knepp, T. N.: Evaluation of OMI operational standard NO_2 column retrievals using in situ and surface-based NO_2 observations, Atmos. Chem. Phys., 14, 11587-11609, doi:10.5194/acp-14-11587-2014, 2014.

Li, Q., Jacob, D. J., Park, R., Wang, Y. Heald, C. L., Hudman, R., Yantosca, R. M.: North American pollution outflow and the trapping of convectively lifted pollution by upper-level anticyclone, J. Geophys. Res., 110, doi:10.1029/2004JD005039, 2005.

Li, X., Rohrer, F., Hofzumahaus, A., Brauers, T., Haseler, R., Bohn, B., Broch, S., Fuchs, H., Gomm, S., Holland, F., Jager, J., Kaiser, J., Keutsch, F. N., Lohse, I., Lu, K., Tillmann, R., Wegener, R., Wolfe, G. M., Mentel, T. F., Kiendler-Scharr, A., and Wahner, A.: Missing gas-phase source of HONO inferred from Zeppelin measurements in the troposphere, Science, 344, 292-296, doi:10.1126/science.1248999, 2014.

Lin, J., Youn, D., Liang, X., and Wuebbles, D.: Global model simulation of summertime U.S. ozone diurnal cycle and its sensitivity to PBL mixing, spatial resolution, and emissions, Atmos. Environ., 42, 8470-8483, doi:10.1016/j.atmosenv.2008.08.012, 2008.

Lin, J.-T., and McElroy, M. B.: Impacts of boundary layer mixing on pollutant vertical profiles in the lower troposphere: Implications to satellite remote sensing, Atmos. Environ., 44, 1726-1739, doi:10.1016/j.atmosenv.2010.02.009, 2010.

Liu, S. C., Trainer, M., Fehsenfeld, F. C., Parrish, D. D., Williams, E. J., Fahey, D. W., Hubler, G., and Murphy, P. C.: Ozone Production in the Rural Troposphere and the Implications for Regional and Global Ozone Distributions, J. Geophys. Res., 92, 4191-4207, 1987.

Liu, Y. J., Herdlinger-Blatt, I., McKinney, K. A., and Martin, S. T.: Production of methyl vinyl ketone and methacrolein via the hydroperoxyl pathway of isoprene oxidation, Atmos. Chem. Phys., 13, 5715-5730, doi:10.5194/acp-13-5715-2013, 2013.

Lu, Z., Streets, D. G., de Foy, B., Lamsal, L. N., Duncan, B. N., and Xing, J.: Emissions of nitrogen oxides from US urban areas: estimation from Ozone Monitoring Instrument retrievals for 2005–2014, Atmos. Chem. Phys., 15, 10367-10383, doi:10.5194/acp-15-10367-2015, 2015.

Mao, J., Jacob, D. J., Evans, M. J., Olson, J. R., Ren, X., Brune, W. H., Clair, J. M. S., Crounse, J. D., Spencer, K. M., Beaver, M. R., Wennberg, P. O., Cubison, M. J., Jimenez, J. L., Fried, A., Weibring, P., Walega, J. G., Hall, S. R., Weinheimer, A. J., Cohen, R. C., Chen, G., Crawford, J. H., McNaughton, C., Clarke, A. D., Jaeglé, L., Fisher, J. A., Yantosca, R. M., Le Sager, P., and Carouge, C.: Chemistry of hydrogen oxide radicals (HO_x) in the Arctic troposphere in spring, Atmos. Chem. Phys., 10, 5823-5838, doi:10.5194/acp-10-5823-2010, 2010.

Mao, J., Paulot, F., Jacob, D. J., Cohen, R. C., Crounse, J. D., Wennberg, P. O., Keller, C. A., Hudman, R. C., Barkley, M. P., and Horowitz, L. W.: Ozone and organic nitrates over the eastern United States: Sensitivity to isoprene chemistry, J. Geophys. Res.: Atmospheres, 118, 11,256-211,268, doi:10.1002/jgrd.50817, 2013.

Marais, E. A., Jacob, D. J., Jimenez, J. L., Campuzano-Jost, P., Day, D. A., Hu, W., Krechmer, J., Zhu, L., Kim, P. S., Miller, C. C., Fisher, J. A., Travis, K., Yu, K., Hanisco, T. F., Wolfe, G. M., Arkinson, H. L., Pye, H. O. T., Froyd, K. D., Liao, J., and McNeil, F. V.: Aqueous-phase mechanism for secondary organic aerosol formation from isoprene: application to the Southeast United States and co-benefit of SO_2 emission controls, Atmos. Chem. Phys., 16, 1603-1618, doi:10.5194/acp-16-1603-2016, 2016.

Martin, R. V., Chance, K., Jacob, D. J., Kurosu, T. P., Spurr, R. J. D., Bucsela, E., Gleason, J. F., Palmer, P. I., Bey, I., Fiore, A. M., Li, Q., Yantosca, R. M., and Koelemeijer, R. B. A.: An improved retrieval of tropospheric nitrogen dioxide from GOME, J. Geophys. Res., 107, doi:10.1029/2001jd001027, 2002.

McDonald-Buller, E. C., Allen, D. T., Brown, N., Jacob, D. J., Jaffe, D., Kolb, C. E., Lefohn, A. S., Oltmans, S., Parrish, D. D., Yarwood, G., and Zhang, L.: Establishing policy relevant background (PRB) ozone concentrations in the United States, Envir. Sci. Tech., 45, 9484-9497, doi:10.1021/es2022818, 2011.

Mena-Carrasco, M., Tang, Y., Carmichael, G. R., Chai, T., Thongbongchoo, N., Campbell, J. E., Kulkarni, S., Horowitz, L., Vukovich, J., Avery, M., Brune, W., Dibb, J. E., Emmons, L., Flocke, F., Sachse, G. W., Tan, D., Shetter, R., Talbot, R. W., Streets, D. G., Frost, G., and Blake, D.: Improving regional ozone modeling through systematic evaluation of errors using the aircraft observations during the International Consortium for Atmospheric Research on Transport and Transformation, J. Geophys. Res., 112, doi:10.1029/2006jd007762, 2007.

Müller, J. F. and Brasseur, G.: Sources of upper tropospheric HO_x: A three-dimensional study, J. Geophs. Res., 104, 1705-1715, 1999.

Murray, L. T., Jacob, D. J., Logan, J. A., Hudman, R. C., and Koshak, W. J.: Optimized regional and interannual variability of lightning in a global chemical transport model constrained by LIS/OTD satellite data, J. Geophys. Res., 117, doi:10.1029/2012jd017934, 2012.

NADP: National Atmospheric Deposition Program (NRSP-3) in: Illinois State Water Survey, edited by: Office, N. P., 2204 Griffith Dr., Champaign, IL 61820., 2007.

NASA, U. G.: OMI/Aura Level 2 Nitrogen Dioxide (NO_2) Trace Gas Column Data 1-Orbit subset Swath along CloudSat track 1-Orbit Swath 13x24 km,version 003 in, edited by: Center, N. G. S. F., 2012.

Nault, B. A., Garland, C., Pusede, S. E., Wooldridge, P. J., Ullmann, K., Hall, S. R., and Cohen, R. C.: Measurements of $CH_3O_2NO_2$ in the upper troposphere, Atmospheric Measurement Techniques, 8, 987-997, doi:10.5194/amt-8-987-2015, 2015.

Nguyen, T. B., Crounse, J. D., Teng, A. P., St Clair, J. M., Paulot, F., Wolfe, G. M., and Wennberg, P. O.: Rapid deposition of oxidized biogenic compounds to a temperate forest, P. Natl. Acad. Sci USA, 112, E392-401, doi:10.1073/pnas.1418702112, 2015.

Ott, L. E., Pickering, K. E., Stenchikov, G. L., Allen, D. J., DeCaria, A. J., Ridley, B., Lin, R.-F., Lang, S., and Tao, W.-K.: Production of lightning NO_x and its vertical distribution calculated from three-dimensional cloud-scale chemical transport model simulations, J. Geophys. Res., 115, doi:10.1029/2009jd011880, 2010.

Palmer, P. I., Jacob, D. J., Chance, K., Martin, R. V., Spurr, R. J. D., Kurosu, T. P., Bey, I., Yantosca, R., Fiore, A., and Li, Q.: Air mass factor formulation for spectroscopic measurements from satellites: Application to formaldehyde retrievals from the Global Ozone Monitoring Experiment, J. Geophys. Res., 106, 14539, doi: 10.1029/2000jd900772, 2001.

Paulot, F., Crounse, J. D., Kjaergaard, H. G., Kroll, J. H., Seinfeld, J. H., and Wennberg, P. O.: Isoprene photooxidation: new insights into the production of acids and organic nitrates, Atmos. Chem. Phys., 9, 1479-1501, 2009a.

Paulot, F., Crounse, J. D., Kjaergaard, H. G., Kurten, A., St Clair, J. M., Seinfeld, J. H., and Wennberg, P. O.: Unexpected Epoxide Formation in the Gas-Phase Photooxidation of Isoprene, Science, 325, 730-733, doi: 10.1126/Science.1172910, 2009b.

Paulot, F., Jacob, D. J., Pinder, R. W., Bash, J. O., Travis, K., and Henze, D. K.: Ammonia emissions in the United States, European Union, and China derived by high-resolution inversion of ammonium wet deposition data: Interpretation with a new agricultural emissions inventory (MASAGE_NH3), J. Geophys. Res.: Atmospheres, 119, 4343-4364, doi:10.1002/2013jd021130, 2014.

Peeters, J., Nguyen, T. L., and Vereecken, L.: HO_x radical regeneration in the oxidation of isoprene, Phys. Chem. Chem. Phys., 11, 5935-5939, doi:10.1039/b908511d, 2009.

Peeters, J., and Müller, J. F.: HO(x) radical regeneration in isoprene oxidation via peroxy radical isomerisations. II: experimental evidence and global impact, Phys. Chem. Chem. Phys., 12, 14227-14235, doi:10.1039/c0cp00811g, 2010.

Peeters, J., Müller, J. F., Stavrakou, T., and Nguyen, V. S.: Hydroxyl radical recycling in isoprene oxidation driven by hydrogen bonding and hydrogen tunneling: the upgraded LIM1 mechanism, J. Phys. Chem.-US. A, 118, 8625-8643, doi:10.1021/jp5033146, 2014.

Pollack, I. B., Lerner, B. M., and Ryerson, T. B.: Evaluation of ultraviolet light-emitting diodes for detection of atmospheric NO_2 by photolysis – chemilumenescence, J. Atmos. Chem., 65(2), 111-125, doi:10.1007/s10874-011-9184-3, 2010.

Prather, M.J., and D.J. Jacob, A persistent imbalance in HO_x and NO_x photochemistry of the upper troposphere driven by deep tropical convection, Geophys. Res. Lett., 24, 3189-3192, 1997.

Reed, C., Evans, M. J., Di Carlo, P., Lee, J. D., and Carpenter, L. J.: Interferences in photolytic NO_2 measurements: explanation for an apparent missing oxidant?, Atmos. Chem. Phys., 16, 4707–4724, doi:10.5194/acp-16-4707-2016, 2016.

Reidmiller, D. R., Fiore, A. M., Jaffe, D. A., Bergmann, D., Cuvelier, C., Dentener, F. J., Duncan, B. N., Folberth, G., Gauss, M., Gong, S., Hess, P., Jonson, J. E., Keating, T., Lupu, A., Marmer, E., Park, R., Schultz, M. G., Shindell,

D. T., Szopa, S., Vivanco, M. G., Wild, O., and Zuber, A.: The influence of foreign vs. North American emissions on surface ozone in the US, Atmos. Chem. Phys., 9, 5027-5042, 2009.

Rickard, A. R., Salisburyg, G., Monks, P. S., Lewis, A. C., Baugitte, S., Bandy, B. J., Clemitshaw, K. C., and Penkett, S. A.: Comparison of Measured Ozone Production Efficiencies in the Marine Boundary Layer at Two European Coastal Sites under Different Pollution Regimes, J. Atmos. Chem., 43, 107-134, 2002.

Russell, A. R., Perring, A. E., Valin, L. C., Bucsela, E. J., Browne, E. C., Wooldridge, P. J., and Cohen, R. C.: A high spatial resolution retrieval of NO_2 column densities from OMI: method and evaluation, Atmos. Chem. Phys., 11, 8543-8554, doi:10.5194/acp-11-8543-2011, 2011.

Russell, A. R., Valin, L. C., and Cohen, R. C.: Trends in OMI NO_2 observations over the United States: effects of emission control technology and the economic recession, Atmos. Chem. Phys., 12, 12197-12209, doi:10.5194/acp-12-12197-2012, 2012.

Ryerson, T. B., Williams, E. J., and Fehsenfeld, F. C.: An efficient photolysis system for fast-response NO_2 measurements, J. Geophys. Res., 105, 26447, doi:10.1029/2000jd900389, 2000.

Ryerson, T. B., Buhr, M. P., Frost, G. J., Goldan, P. D., Holloway, J. S., Hübler, G., Jobson, B. T., Kuster, W. C., McKeen, S. A., Parrish, D. D., Roberts, J. M., Sueper, D. T., Trainer, M., Williams, J. and Fehsenfeld, F. C.: Emissions lifetimes and ozone formation in poewr plant plumes, J. Geophys. Res., 103*(D17)*, 22569-22583, 1998.

Sander, S. P., Abbatt, J., Barker, J. R., Burkholder, J. B., Friedl, R. R., Golden, D. M., Huie, R. E., Kolb, C. E., Kurylo, M. J., Moortgat, G. K., Orkin, V. L., and Wine, P. H.: Chemical Kinetics and Photochemical Data for Use in Atmospheric Studies, Evaluation No. 17, in, JPL Publication 10-6, Jet Propulsion Laboratory, Pasadena, 2011.

Schultz, M. G., Jacob, D. J., Wang, Y., Logan, J. A., Atlas, E. L., Blake, D. R., Blake, N. J., Bradshaw, J. D., Browell, E. V., Fenn, M. A., Flocke, F., Gregory, G. L., Heikes, B. G., Sachse, G. W., Sandholm, S. T., Shetter, R. E., Singh, H. B., and Talbot, R. W.: On the origin of tropospheric ozone and NO_x over the tropical South Pacific, J. Geophys. Res., 104, 5829, doi:10.1029/98jd02309, 1999.

Shetter, R. E., and Muller, M.: Photolysis frequency measurements using actinic flux spectroradiometry during the PEM-Tropics mission: Instrumentation description and some results, J. Geophys. Res., 104, 5647-5661, doi:10.1029/98JD01381, 1999.

Singh, H. B., Brune, W. H., Crawford, J. H., Jacob, D. J., and Russell, P. B.: Overview of the summer 2004 Intercontinental Chemical Transport Experiment–North America (INTEX-A), J. Geophys. Res., 111, doi:10.1029/2006jd007905, 2006.

Squire, O. J., Archibald, A. T., Griffiths, P. T., Jenkin, M. E., Smith, D., and Pyle, J. A.: Influence of isoprene chemical mechanism on modelled changes in tropospheric ozone due to climate and land use over the 21st century, Atmos. Chem. Phys., 15, 5123-5143, doi:10.5194/acp-15-5123-2015, 2015.

St. Clair, J. M., Rivera-Rios, J. C., Crounse, J. D., Knap, H. C., Bates, K. H., Teng, A. P., Jorgensen, S., Kjaergaard, H. G., Keutsch, F. N., and Wennberg, P. O.: Kinetics and Products of the Reaction of the First-Generation Isoprene Hydroxy Hydroperoxide (ISOPOOH) with OH, J. Phys. Chem.-US. A, doi:10.1021/acs.jpca.5b06532, 2015.

St. Clair, J. M., McCabe, D. C., Crounse, J. D., Steiner, U., and Wennberg, P. O.: Chemical ionization tandem mass spectrometer for the in situ measurement of methyl hydrogen peroxide, Rev. Sci. Instrum., 81, doi:10.1063/1.3480552, 2010.

Stavrakou, T., Peeters, J., and Müller, J. F.: Improved global modelling of HO_x recycling in isoprene oxidation: evaluation against the GABRIEL and INTEX-A aircraft campaign measurements, Atmos. Chem. Phys., 10, 9863-9878, doi:10.5194/acp-10-9863-2010, 2010.

Toon, O. B., Maring, H., Dibb, J., Ferrare, R., Jacob, D. J., Jensen, E. J., Luo, Z. J., Mace, G. G., Pan, L. L., Pfister, L., Rosenlof, K. H., Redemann, J., Reid, J. S., Singh, H. B., Yokelson, R. J., Minnis, P., Chen, G., Jucks, K. W., and Pszenny, A.: Planning, implementation, and scientific goals of the Studies of Emissions and Atmospheric Composition, Clouds, and Climate Coupling by Regional Surveys (SEAC4RS) field mission, J. Geophys. Res., in review, 2016.

Trainer, M., Parrish, D. D., Buhr, M. P., Norton, R. B., Fehsenfeld, F. C., Anlauf, K. G., Bottenheim, J. W., Tang, Y. Z., Wiebe, H. A., Roberts, J. M., Tanner, R. L., Newman, L., Bowersox, C., Meagher, J. F., Olszyna, K. J., Rodgers, M. O., Wang, T., Berresheim, H., Demerjian, K. L., and Roychowdhury, U. K.: Correlation of ozone with NO_y in photochemically aged air, J. Geophys. Res., 98, 2917-2925, 1993.

Trainer, M., Parrish, D. D., Goldan, P. D., Roberts, J., and Fehsenfeld, F. C.: Review of observation-based analysis of the regional factors influencing ozone concentrations, Atmos. Environ., 34, 2045-2061, 2000.

Vinken, G. C. M., Boersma, K. F., Maasakkers, J. D., Adon, M., and Martin, R. V.: Worldwide biogenic soil NO_x emissions inferred from OMI NO_2 observations, Atmos. Chem. Phys., 14, 10363-10381, doi:10.5194/acp-14-10363-2014, 2014.

Walker, T. W.: Applications of Adjoint Modeling in Chemical Composition: Studies of Tropospheric Ozone at Middle and High Northern Latitudes, Graduate Department of Physics, University of Toronto, 2014.

Wang, Y., Jacob, D. J., and Logan, J. A.: Global simulation of tropospheric O3-NOx-hydrocarbon chemistry, 1. Model formulation, J. Geophys. Res., 103, 10,727-710,755, 1998.

Wesely, M. L.: Parameterization of Surface Resistances to Gaseous Dry Deposition in Regional-Scale Numerical-Models, Atmos. Environ., 23, 1293-1304, doi:10.1016/0004-6981(89)90153-4, 1989.

Wolfe, G. M., Crounse, J. D., Parrish, J. D., St Clair, J. M., Beaver, M. R., Paulot, F., Yoon, T. P., Wennberg, P. O., and Keutsch, F. N.: Photolysis, OH reactivity and ozone reactivity of a proxy for isoprene-derived hydroperoxyenals (HPALDs), Phys. Chem. Chem. Phys., 14, 7276-7286, doi:10.1039/c2cp40388a, 2012.

Wolfe, G. M., Hanisco, T. F., Arkinson, H. L., Bui, T. P., Crounse, J. D., Dean-Day, J., Goldstein, A., Guenther, A., Hall, S. R., Huey, G., Jacob, D. J., Karl, T., Kim, P. S., Liu, X., Marvin, M. R., Mikoviny, T., Misztal, P. K., Nguyen, T. B.,

Peischl, J., Pollack, I., Ryerson, T., St. Clair, J. M., Teng, A., Travis, K. R., Ullman, K., Wennberg, P. O., and Wisthaler, A.: Quantifying Sources and Sinks of Reactive Gases in the Lower Atmosphere using Airborne Flux Observations, Geophys. Res. Lett., 42, 8231-8240, doi:10.1002/2015GL065839, 2015.

Xie, Y., Paulot, F., Carter, W. P. L., Nolte, C. G., Luecken, D. J., Hutzell, W. T., Wennberg, P. O., Cohen, R. C., and Pinder, R. W.: Understanding the impact of recent advances in isoprene photooxidation on simulations of regional air quality, Atmos. Chem. Phys., 13, 8439-8455, doi:10.5194/acp-13-8439-2013, 2013.

Yu, K., Jacob, D. J., Fisher, J. A., Kim, P. S., Marais, E. A., Miller, C. C., Travis, K. R., Zhu, L., Yantosca, R. M., Sulprizio, M. P., Cohen, R. C., Dibb, J. E., Fried, A., Mikoviny, T., Ryerson, T. B., Wennberg, P. O., and Wisthaler, A.: Sensitivity to grid resolution in the ability of a chemical transport model to simulate observed oxidant chemistry under high-isoprene conditions, Atmos. Chem. Phys., 16, 4369–4378, doi:10.5194/acp-16-4369-2016, 2016.

Zaveri, R. A.: Ozone production efficiency and NO_x depletion in an urban plume: Interpretation of field observations and implications for evaluating O3-NO_x-VOC sensitivity, J. Geophys. Res., 108, doi:10.1029/2002jd003144, 2003.

Zhang, L., Jacob, D., J., Yue, X., Downey, N. V., Wood, D. A., Blewitt, D., Sources contributing to background surface ozone in the US Intermountain West, Atmos. Chem. Phys., 14, 5295-5309, doi:10.5194/acp-14-5295-2014, 2014.

Zhou, X., Ye, C., Pu, D., Stutz, J., Festa, J., Spolaor, M., Weinheimer, A. J., Campos, T. L., Haggerty, J. A., Cantrell, C. A., Mauldin, L., Guenther, A. B., Hornbrook, R. S., Apel, E. C., and Jensen, J. B.: Tropospheric HONO Distribution and Chemistry in the Southeastern US, American Geophysical Union, Fall Meeting 2014, 2014.

Zhu, L., Jacob, D. J., Mickley, L. J., Kim, P. S., Fisher, J. A., Travis, K. R., Yu, K., Yantosca, R. M., Sulprizio, M. P., Fried, A., Hanisco, T., Wolfe, G., Abad, G. G., Chance, K., De Smedt, I., and Yang, K.: Observing atmospheric formaldehyde (HCHO) from space: validation and intercomparison of six retrievals from four satellites (OMI, GOME2A, GOME2B, OMPS) with SEAC^{4}RS aircraft observations over the Southeast US, Atmos. Chem. Phys. Discussions, doi:10.5194/acp-2016-162, 2016.

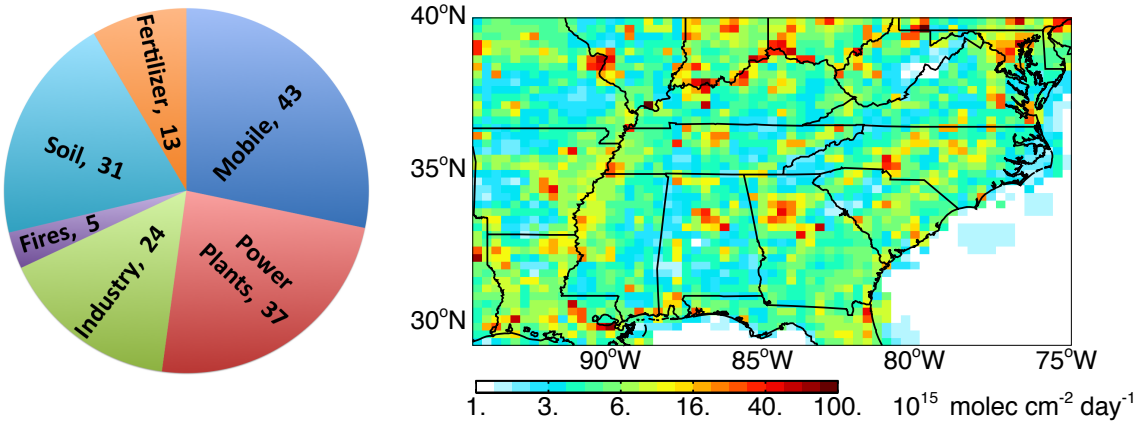

Figure 1: Surface NO_x emissions in the Southeast US in GEOS-Chem for August and September 2013 including fuel combustion, soils, fertilizer use, and open fires (total emissions=153 Gg N). Anthropogenic emissions from mobile sources and industry in the National Emission Inventory (NEI11v1) for 2013 have been decreased by 60% to match atmospheric observations (see text). Lightning contributes an additional 25 Gg N to the free troposphere (not included in the Figure). The emissions are mapped on the 0.25° × 0.3125° GEOS-Chem grid. The pie chart gives the sum of August-September 2013 emissions (Gg N) over the Southeast US domain as shown on the map (94.5 - 75° W, 29.5-40° N).

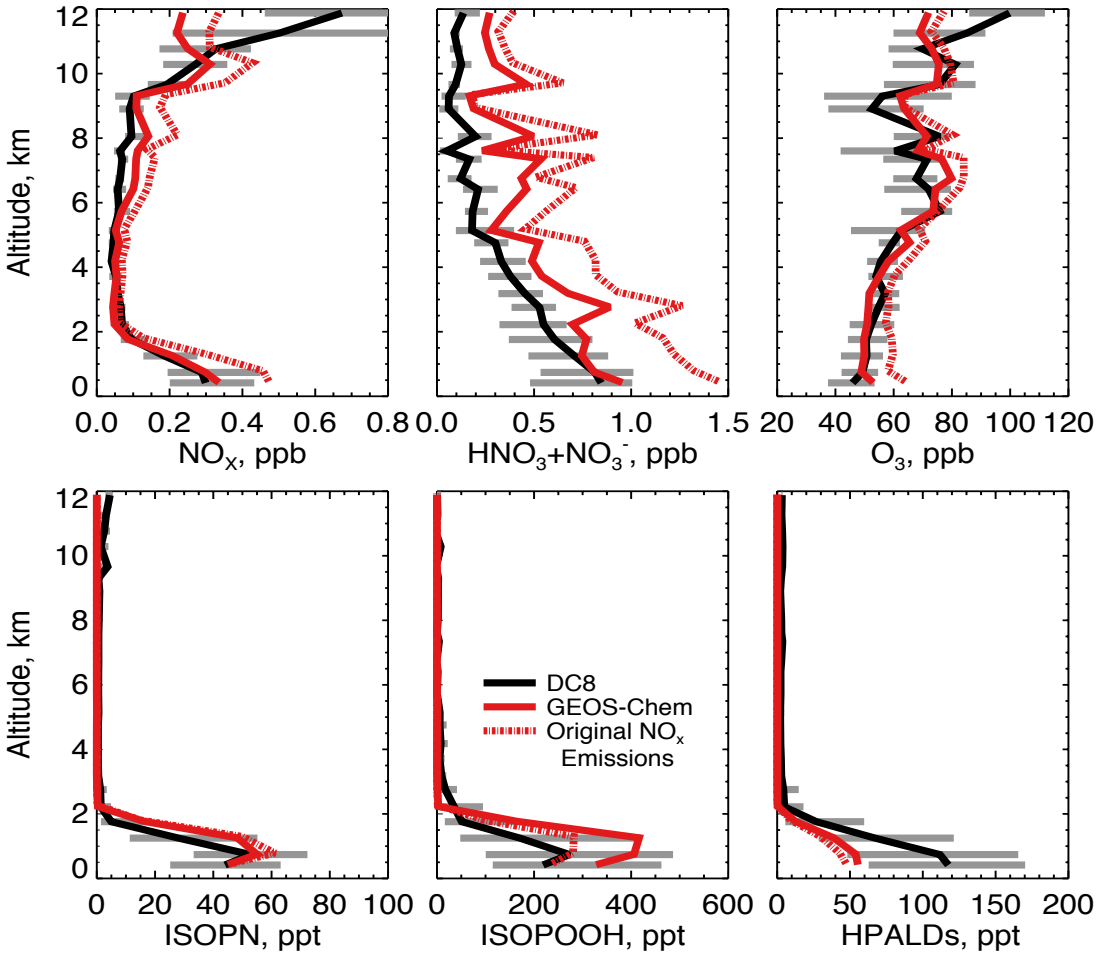

Figure 2: Median vertical concentration profiles of NO_x, total inorganic nitrate (gas HNO_3+ aerosol NO_3^-), ozone, isoprene nitrate (ISOPN), isoprene hydroperoxide (ISOPOOH), and hydroperoxyaldehydes (HPALD) for the SEAC^{4}RS flights over the Southeast US (domain of Figure 1). Observations from the DC-8 aircraft are compared to GEOS-Chem model results. The dashed red line shows model results before adjustment of NO_x emissions from fuel combustion and lightning (see text). The 25th and 75th percentiles of the DC-8 observations are shown as grey bars. The SEAC^{4}RS observations have been filtered to remove open fire plumes, stratospheric air, and urban plumes as described in the text. Model results are sampled along the flight tracks at the time of flights and gridded to the model resolution. Profiles are binned to the nearest 0.5 km. The NOAA NO_yO_3 4-channel chemiluminescence (CL) instrument made measurements of ozone and NO_y (Ryerson et al., 1998), NO (Ryerson et al., 2000) and NO_2 (Pollack et al, 2010). Total inorganic nitrate was measured by the University of New Hampshire Soluble Acidic Gases and Aerosol (UNH SAGA) instrument (Dibb et al., 2003) and was mainly gas-phase HNO_3 for the SEAC^{4}RS conditions. ISOPOOH, ISOPN, and HPALDs were measured by the Caltech single mass analyzer CIMS (Crounse et al., 2006; Paulot et al., 2009a; Crounse et al., 2011).

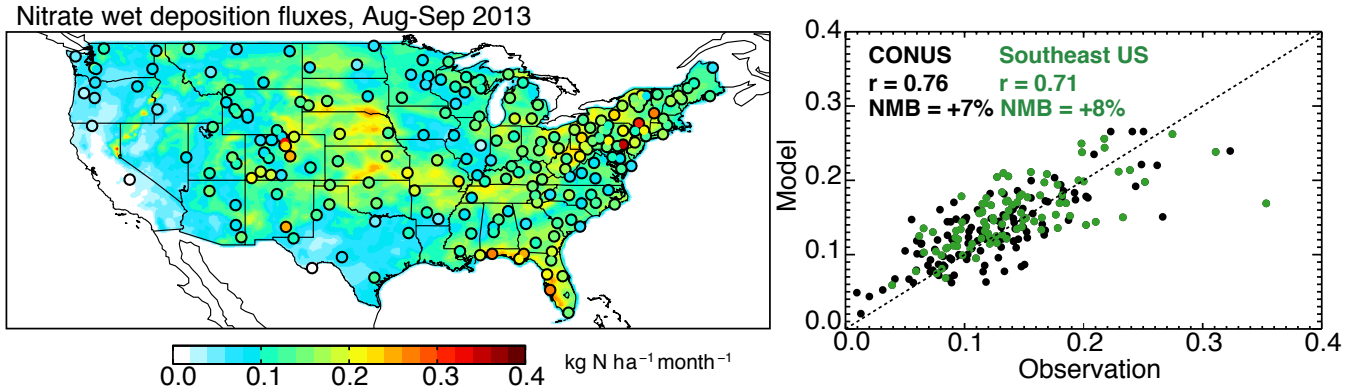

Figure 3: Nitrate wet deposition fluxes across the US in August-September 2013. Mean observations from the NADP network (circles in the left panel) are compared to model values with decreased NO_x emissions (background). Also shown is a scatterplot of simulated versus observed values at individual sites for the whole contiguous US (black) and for the Southeast US (green). The correlation coefficient (*r*) and normalized mean bias (NMB) are shown inset, along with the 1:1 line.

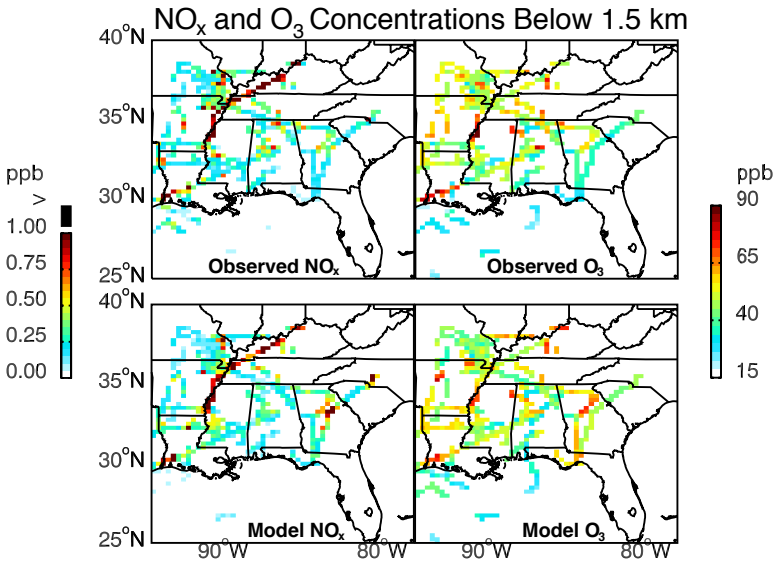

Figure 4: Ozone and NO_x concentrations in the boundary layer (0-1.5km) during SEAC^{4}RS (6 Aug to 23 Sep 2013) Observations from the aircraft and simulated values are averaged over the 0.25°x0.3125° GEOS-Chem grid. NO_x above 1ppb is shown in black. The spatial correlation coefficient is 0.71 for both NO_x and O_3. The normalized mean bias is -11.5% for NO_x and 4.5% for O_3.

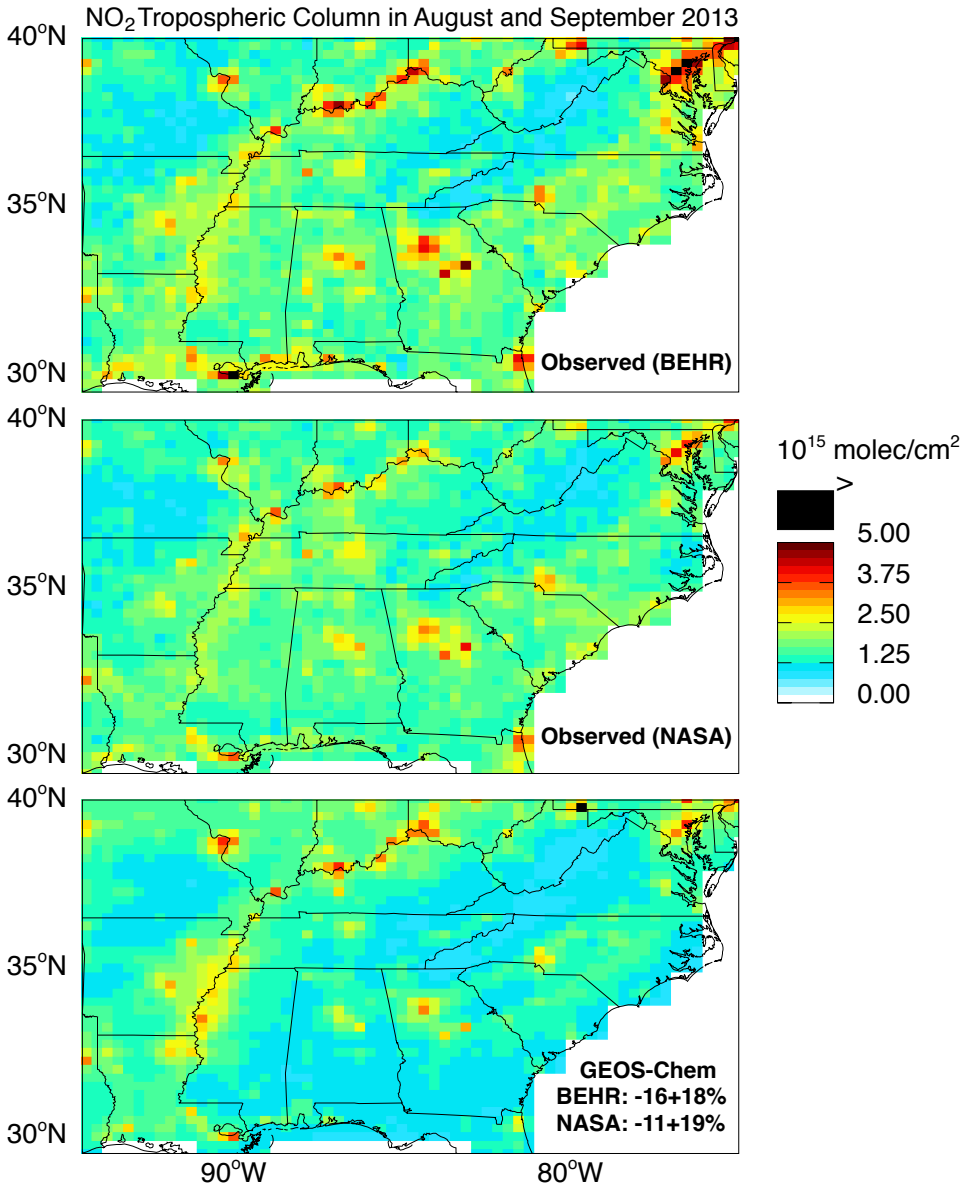

Figure 5: NO_2 tropospheric columns over the Southeast US in August-September 2013. GEOS-Chem (sampled at the 13:30 local time overpass of OMI) is compared to OMI satellite observations using the BEHR and NASA retrievals. Values are plotted on the 0.25^ox0.3125^o GEOS-Chem grid. The GEOS-Chem mean bias over the Figure domain and associated spatial standard deviation are inset in the bottom panel.

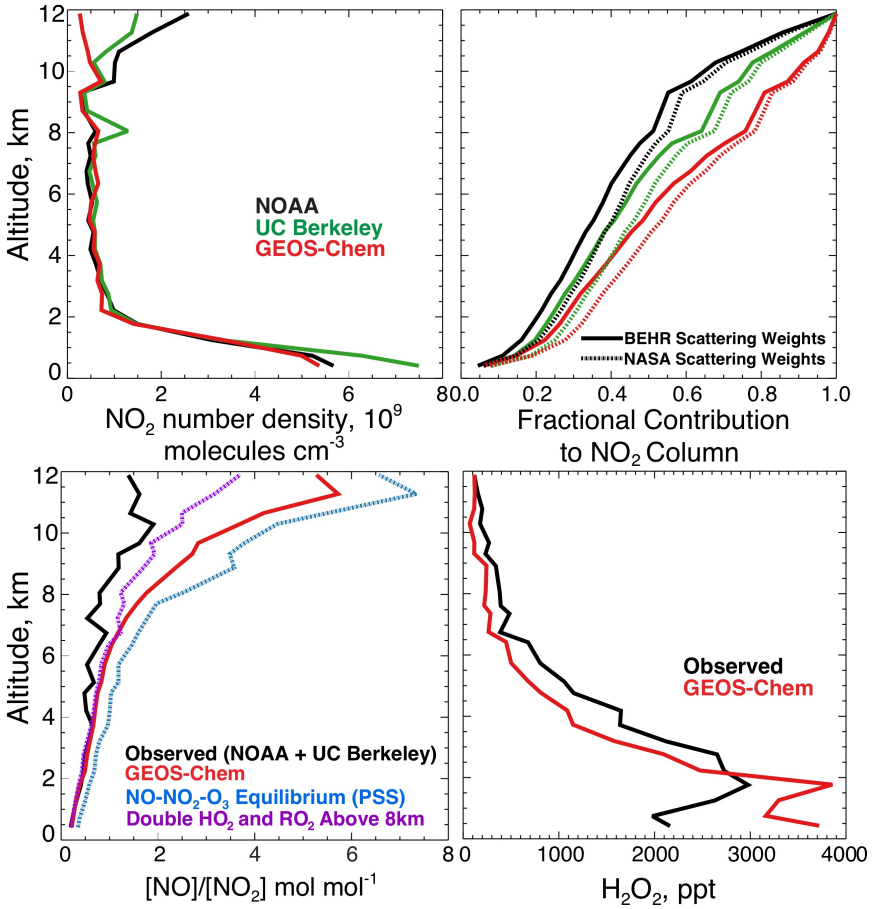

Figure 6: Vertical distribution of NO_2 over the Southeast US during SEAC^{4}RS (August-September 2013) and contributions to tropospheric NO_2 columns measured from space by OMI. The top left panel shows median vertical profiles of NO_2 number density measured from the SEAC^{4}RS aircraft by the NOAA and UC Berkeley instruments and simulated by GEOS-Chem. The top right panel shows the fractional contribution of NO_2 below a given altitude to the total tropospheric NO_2 slant column measured by OMI, accounting for increasing sensitivity with altitude as determined from the retrieval scattering weights. The bottom left panel shows the median vertical profiles of the daytime [NO]/[NO_2] molar concentration ratio in the aircraft observations (NOAA for NO and UC Berkeley for NO_2) and in GEOS-Chem. Also shown is the ratio computed from NO-NO_2-O_3 photochemical steady state (PSS) as given by reactions (5)+(7) (blue) and including reaction (6) with doubled HO_2 and RO_2 concentrations above 8km (purple). The bottom right panel shows the median H_2O_2 profile from the model and from the SEAC4RS flights over the Southeast US. H_2O_2 was measured by the Caltech CIMS (see Figure 2).

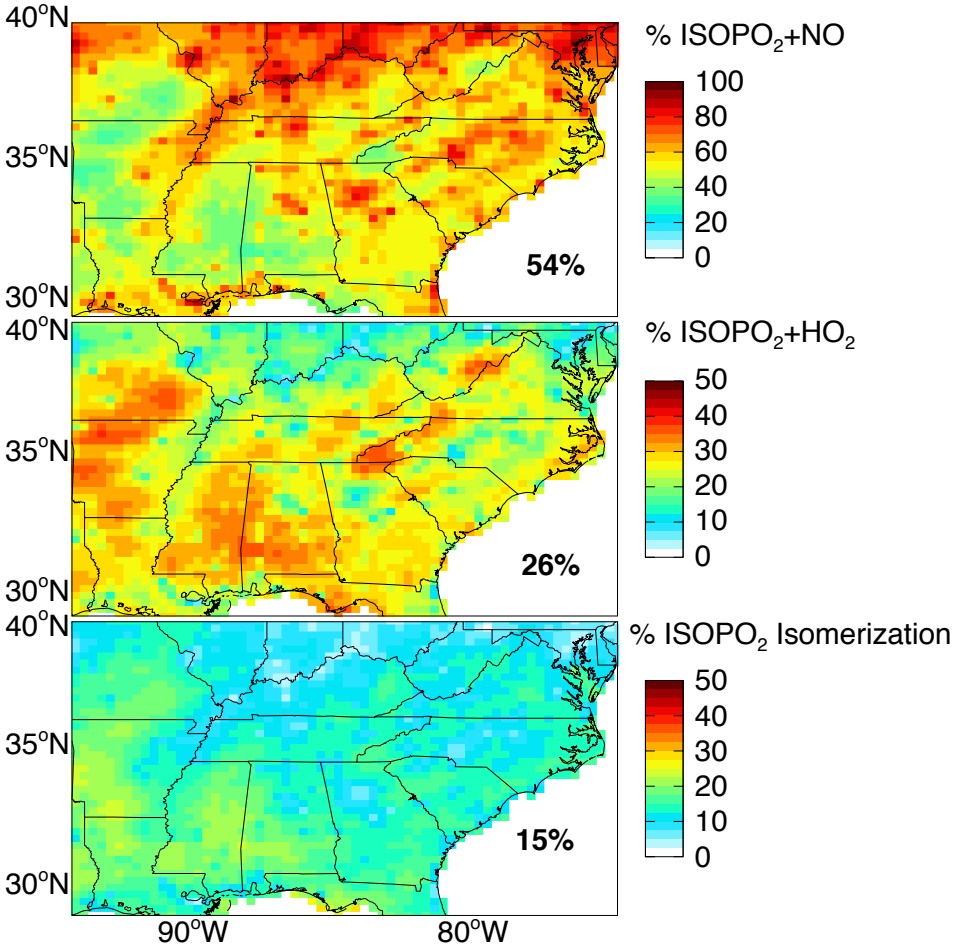

Figure 7: Branching ratios for the fate of the isoprene peroxy radical ($ISOPO_2$) as simulated by GEOS-Chem over the Southeast US for August-September 2013. Values are percentages of $ISOPO_2$ that react with NO, HO_2, or isomerize from the total mass of isoprene reacting over the domain. Note the difference in scale between the top panel and the lower two panels. Regional mean percentages for the Southeast US are shown inset. They add up to less than 100% because of the small $ISOPO_2$ sink from reaction with other organic peroxy radicals (RO_2).

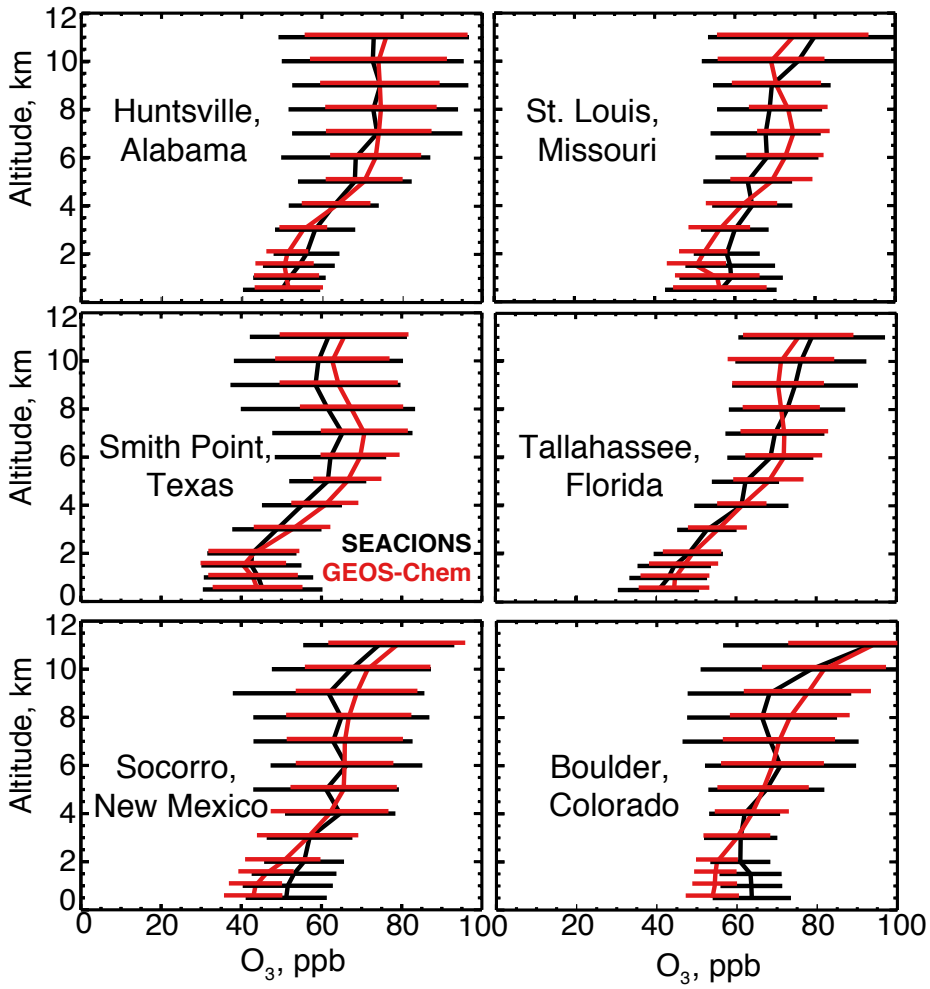

Figure 8: Mean ozonesonde vertical profiles at the US SEACIONS sites (http://croc.gsfc.nasa.gov/seacions/) during the SEAC^{4}RS campaign in August-September 2013. An average of 20 sondes were launched per site between 9am and 4pm local time. Ozonesondes at Smith Point, Texas were only launched in September. Model values are coincident with the launches. Data are averaged vertically over 0.5 km bins below 2 km altitude and 1.0 km bins above. Also shown are standard deviations.

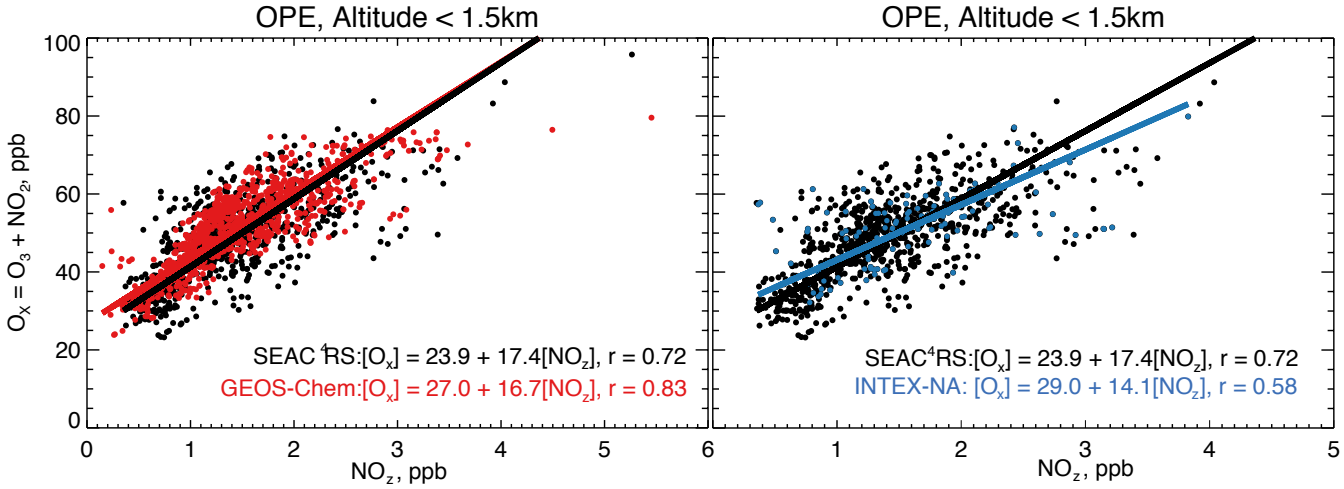

Figure 9: Ozone production efficiency (OPE) over the Southeast US in summer estimated from the relationship between odd oxygen (O_x) and the sum of NO_x oxidation products (NO_z) below 1.5 km altitude. The left panel compares SEAC^{4}RS observations to GEOS-Chem values for August-September 2013 (data from Figure 2). The right panel compares SEAC^{4}RS observations to INTEX-NA aircraft observations collected over the same Southeast US domain in summer 2004 (Singh et al., 2006). NO_z is defined here as HNO_3 + PAN + alklynitrates, all of which were measured from the SEAC^{4}RS and INTEX-NA aircraft. The slope and intercept of the reduced-major-axis (RMA) regression are provided inset with the correlation coefficient (r). Observations for INTEX-NA were obtained from ftp://ftp-air.larc.nasa.gov/pub/INTEXA/.

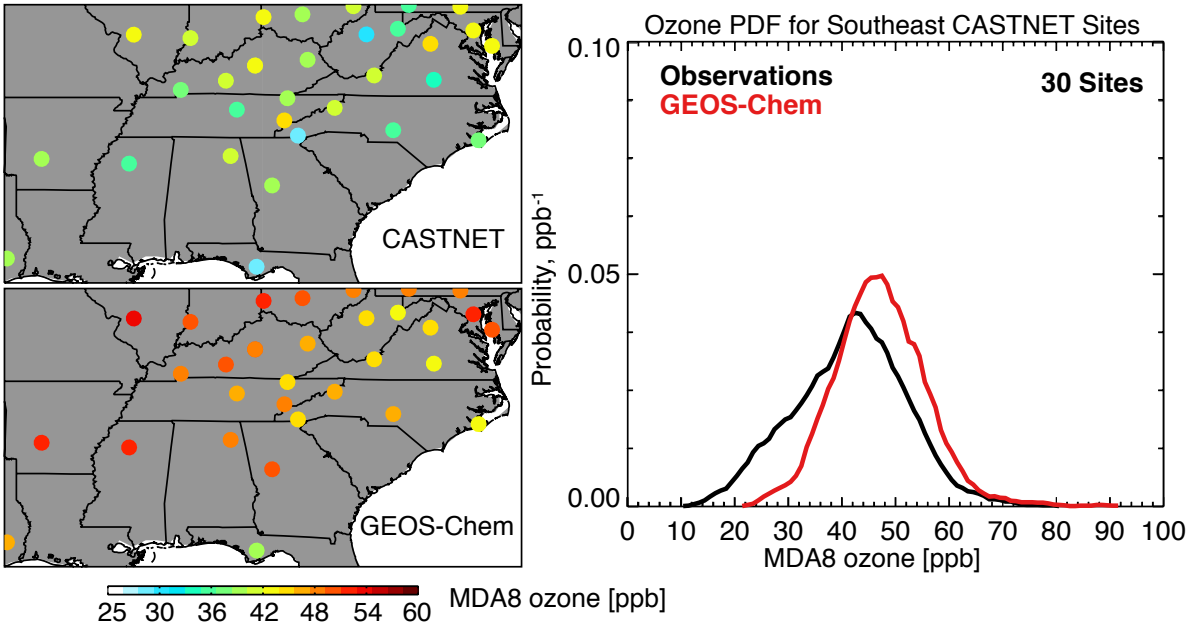

Figure 10: Maximum daily 8-h average (MDA8) ozone concentrations at the 30 CASTNET sites in the Southeast US in June-August 2013. The left panels show seasonal mean values in the observations and GEOS-Chem. The right panel shows the probability density functions (pdfs) of daily values at the 30 sites.

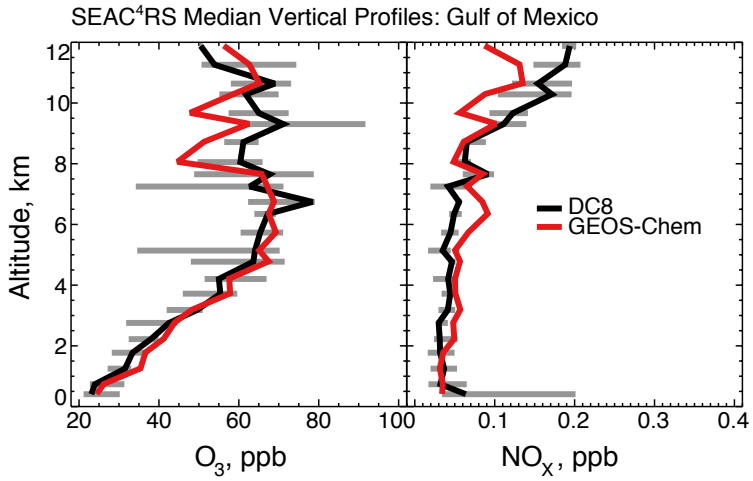

Figure 11: Median vertical profiles of ozone and NO_x concentrations over the Gulf of Mexico during SEAC^{4}RS. Observations are from four SEAC^{4}RS flights over the Gulf of Mexico (August 12, September 4, 13, 16). GEOS-Chem model values are sampled along the flight tracks. The 25th and 75th percentiles of the aircraft observations are shown as horizontal bars.

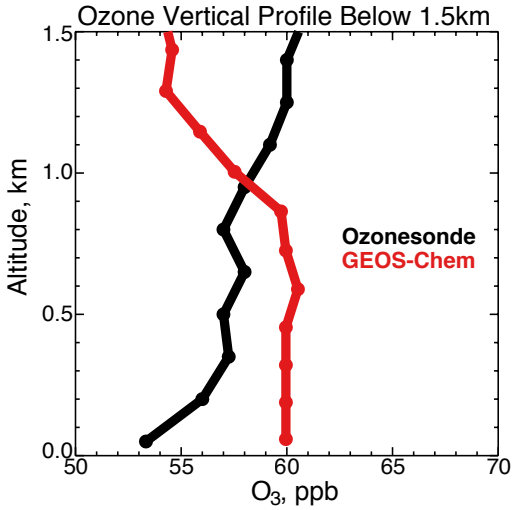

Figure 12: Median vertical profile of ozone concentrations over St. Louis, Missouri and Huntsville, Alabama during August and September 2013. Observations from SEACIONS ozonesondes launched between 10 and 13 local time (57 launches) are compared to GEOS-Chem results sampled at the times of the ozonesonde launches and at the vertical resolution of the model (11 layers below 1.5km, red circles). The ozonesonde data are shown at 150m resolution. Altitude is above local ground level.